A complete Thermo-Electro-Viscoelastic Characterization of Dielectric Elastomers - Part II: Continuum Modelling Approach

Markus Mehnert, Mokarram Hossain and Paul Steinmann

Abstract A comprehensive experimental study performed under a combination of thermo-electro-mechanical loads applied to a widely used electro-active polymer, is presented in the Part I of this work (Mehnert et al., submitted, 2021). Soft polymeric materials, used as base materials in electro-active polymers, are highly susceptible to temperature changes. Hence, thermal influences on their behavior have to be investigated precisely. Constitutive modelling and numerical simulation of electro-active polymers are active fields of current research. However, on the one hand, their experimental study under complex loading conditions is non-trivial. On the other hand, very few constitutive modelling approaches meet with experimental data obtained from thermo-electro-mechanical loading conditions. In this contribution, we aim to develop a thermo-electro-mechanically coupled model, which will closely replicate the response of an electro-active polymer investigated under a combination of thermal, electric and mechanical loads. Once the model is calibrated with the experimental data described in Part I of this contribution, it is validated with a different set of data, which shows excellent agreement with experimental findings.

Markus Mehnert
Institute of Applied Mechanics, University of Erlangen-Nuremberg, Egerlandstr. 5, 91058 Erlangen, Germany, e-mail: markus.mehnert@fau.de

Paul Steinmann
Institute of Applied Mechanics, University of Erlangen-Nuremberg, Egerlandstr. 5, 91058 Erlangen, Germany e-mail: paul.steinmann@fau.de
Glasgow Computational Engineering Centre (GCEC), University of Glasgow, United Kingdom

Mokarram Hossain
Zienkiewicz Centre for Computational Engineering, College of Engineering, Bay Campus, Swansea University, Swansea, UK e-mail: mokarram.hossain@swansea.ac.uk

1 Introduction

'Can materials act as machines?' is one of the most pressing questions among material scientists and engineers since the last decade of the twentieth century [1]. Machines consisting of a set of materials are usually designed to perform some specific tasks such as generating motion or lifting an object. One of the most active field of current research is synthesis and design of responsive materials that can integrate within machines or act as machines. Responsive materials are smart and innovative substances that can be activated under the application of external or internal stimuli including electric field, magnetic field, pH, light, temperature, humidity or combinations of two or more of them. Among others, electro-active polymers (EAPs) are widely accepted, low-cost, responsive materials. EAPs are a group of polymeric materials that can potentially undergo large deformations and can change their attributes when subjected to an electric field. In the development of actuators, adaptable optics or generators, electro-active polymers may complement or even outperform traditional technologies, such as electro-magnetic motors or piezoelectrics [2, 3]. Dielectric elastomers (DEs) are a special subclass of electro-active polymers, which enable the simple design of soft actuators. A dielectric elastomer can be produced when a thin film of a soft polymeric material is sandwiched between two compliant electrodes and it can deform upon the application of an electric potential difference between the electrodes [4]. For the applications of electro-active polymers, it should be taken into account, however, that their base materials are highly sensitive to temperature changes.

An important factor to increase the usability of electro-active polymers is the development of a rigorous continuum modeling and simulation approach allowing to fully harness their potential. The simulation of electro-mechanical material behavior demands for an appropriate coupling of the mechanical description with the theory of electrodynamics. For a comprehensive description of the physical background of electrodynamics, the reader is referred to the standard works of Griffith [5] or Jackson [6]. Early attempts describing the interplay between a deforming body and an electric field can be found in the works of, e.g., Eringen [7] or Toupin [8]. These ground works have been expanded over the last decades specifically sparked by the growing interest in electro-active polymeric materials [9, 10, 11]. Of special importance for the simulation of a wide range of polymeric materials is the consideration of their time-dependent response. For this purpose, numerous material models have been developed that may be characterized by the origin of their time-dependent stress contributions, which are frequently formulated based either on stress-type internal variables [12, 13, 14] or strain-type internal variables [15, 16]. A successful combination of electro-mechanics and viscoelasticity for the simulation of electro-active polymers can be found for example in the works of Ask et al. [17, 18]. After model formulation, their viscoelastic material model was fitted to experimental data of a polyurethane-type elastomer that were obtained from experiments performed under an electro-mechanically coupled loading condition.

As a number of polymers show a significant sensitivity towards temperature changes [19, 20], thermal influences on their behavior should be considered thoroughly.

While polymeric materials are frequently assumed to be incompressible at constant temperature [21], a change in temperature leads to a volumetric deformation of the material due to thermal expansion. Depending on the thermal expansion coefficient of the respective material, these deformations can change the volume of the material up to 5 % for temperature changes in the range of 100 K [20]. Furthermore, the mechanical material parameters can be assumed to be temperature dependent, frequently exhibiting a pronounced softening of the material at increased temperatures [22, 23]. In early attempts of incorporating thermal influences into viscoelastic material models the Time-Temperature-Superposition Principle was used [19], which is, however, only valid for thermo-rheologically simple materials that can be modelled within small strain theories. More general frameworks were presented for example by Lion [24], Reese and Govindjee [25], Behnke et al. [22, 26], Johlitz et al. [27], Dippel et al. [23] or Anand et al. [28, 29].
The focus of Part II is the mathematical and numerical treatment of thermo-electro-mechanical problems in the geometrically nonlinear context. Once mathematical formulations are set-up, experimental data, that was obtained by performing experiments on a classical electro-active polymer, will be utilized. At first, all material parameters appearing in the constitutive model will be identified by a given sub-set of data. Afterwards, for the model validation, independent sets of data will be used that are not part of the parameter identification process.
The work is organized as follows: in Section 2 the required kinematic expressions, balance equations and constitutive equations are introduced as a basis for the thermo-electro-viscoelastic material model that is presented in Section 3. This includes a specified constitutive model for the thermo-electro-viscoelastic material behavior of the dielectric polymer under investigation. In Section 4, the available results from the experiments are combined with the proposed material model in order to identify a set of material parameters describing the response of the dielectric elastomer VHB 4905^{TM}. The paper is closed by some concluding remarks.

2 Constitutive modelling

In this Section, the thermo-electro-mechanical modeling approach is presented and specified with suitable terms from the literature. These are selected in such a way that the material behavior of VHB 4905^{TM} can be replicated as closely as possible with a reasonable amount of material parameters. The reader should note that the description of the presented terms here is deliberately kept short and is layed out in more detail in the corresponding chapters of the Appendix.

2.1 Kinematics

In order to consider the combined influence of electric, mechanical, and thermal loads, a multiplicative decomposition of the deformation gradient $\boldsymbol{F}$ into a thermal part $\boldsymbol{F}_\Theta$ and an electro-mechanical deformation $\boldsymbol{F}_{EM}$ is introduced as

$$\boldsymbol{F} = \boldsymbol{F}_\Theta \boldsymbol{F}_{EM}. \tag{1}$$

The aforementioned decomposition can be interpreted as the introduction of a purely electro-mechanical intermediate configuration, on which quantities can be formulated that are independent of the electro-mechanically induced deformation (c.f. Figure 1).

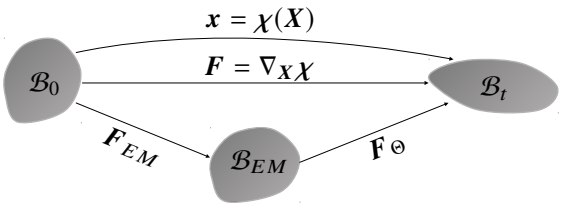

Fig. 1 Introduction of the intermediate configuration $\mathcal{B}_{EM}$ and corresponding decomposition of the total deformation gradient $\boldsymbol{F}$ into an electro-mechanical $\boldsymbol{F}_{EM}$ and a thermal contribution $\boldsymbol{F}_\Theta$.

For more details about this approach, see Lu and Pister [30], Reese and Govindjee [25], Lion [31], Erbts et al. [32]. While $\boldsymbol{F}_\Theta$ is assumed to be purely volumetric, the electro-mechanical deformation may in general combine both volumetric and isochoric deformations. For the latter, a further multiplicative decomposition is frequently used to capture the time-dependent viscoelastic response at finite strains. Thus, the deformation gradient is ultimately decomposed into

$$\boldsymbol{F} = \boldsymbol{F}_\Theta \boldsymbol{F}_{EM} = \boldsymbol{F}_\Theta \boldsymbol{F}^{\text{vol}}_{EM} \boldsymbol{F}^{\text{iso}}_{EM} = \boldsymbol{F}_\Theta \boldsymbol{F}^{\text{vol}}_{EM} \boldsymbol{F}^{e}_{EM} \boldsymbol{F}^{v}_{EM}. \tag{2}$$

Note that the viscous response is assumed to be isochoric only, see Reese and Govindjee [16], Dippel et al. [23]. Furthermore, we can use the deformation gradient $\boldsymbol{F}$ for the definition of the right Cauchy-Green tensor $\boldsymbol{C} = \boldsymbol{F}^T \boldsymbol{F}$. The corresponding elastic and inelastic right Cauchy-Green strain tensors are defined as $\boldsymbol{C}^e_{EM} = [\boldsymbol{F}^e_{EM}]^T \boldsymbol{F}^e_{EM}$ and $\boldsymbol{C}^v_{EM} = [\boldsymbol{F}^v_{EM}]^T \boldsymbol{F}^v_{EM}$, respectively. We introduce the thermal expansion coefficient α and the temperature difference ($\Delta\Theta = \Theta - \Theta_0$) and consider the decomposition of the Jacobian determinant into

$$J = \det \boldsymbol{F} = \det \boldsymbol{F}_\Theta \ \det \boldsymbol{F}_{EM} = J_\Theta J_{EM}, \tag{3}$$

where the thermal Jacobian is expressed either with an exponential function as $J_\Theta = \exp(3\alpha\Delta\Theta)$ or with a linear function, i.e., $J_\Theta = \alpha[\Delta\Theta] + 1$, see Dippel et al.

[23], Erbts et al. [32]. If we assume the material under investigation to be isotropic, the thermal deformation gradient $\boldsymbol{F}_\Theta$ and the corresponding right Cauchy-Green tensor read

$$\boldsymbol{F}_\Theta = J_\Theta^{\frac{1}{3}} \boldsymbol{I} \rightarrow \boldsymbol{C}_\Theta = J_\Theta^{\frac{2}{3}} \boldsymbol{I}. \tag{4}$$

Furthermore, the definition of the isochoric right Cauchy-Green tensor is $\overline{\boldsymbol{C}} = J^{-\frac{2}{3}} \boldsymbol{C}$. As the thermal expansion is purely volumetric, it holds that the isochoric Cauchy-Green tensor capturing the combined deformation is equal to the mechanical contribution, i.e.

$$\overline{\boldsymbol{C}} = \overline{\boldsymbol{C}}_{EM}. \tag{5}$$

Finally, as rubber-like materials can be assumed to be incompressible at a constant temperature, the decomposition into mechanical and thermal deformation resembles a decomposition into a purely isochoric and a purely volumetric deformation. In this case, we can state that

$$\overline{\boldsymbol{C}} = \boldsymbol{C}_{EM} \quad \text{with} \quad J_{EM} = 1 \quad \text{and} \quad J = J_\Theta. \tag{6}$$

2.2 Balance equations

In the presence of matter, the constitutive relation between an electric field $\mathbb{E}$ and the electric displacement in the material configuration reads $\mathbb{D} = \varepsilon_0 J \boldsymbol{C}^{-1} \cdot \mathbb{E} + \mathbb{P}$, with the electric polarization $\mathbb{P}$ and the electric permittivity of vacuum $\varepsilon_0 = 8.85 \times 10^{-12}$ F/m. In the absence of matter, the polarization vanishes and we can define the vacuum electric displacement $\mathbb{D}^\varepsilon := \varepsilon_0 J \boldsymbol{C}^{-1} \cdot \mathbb{E}$. The behavior of the electric field in the material configuration is governed by the Maxwell equations, which take the form

$$\text{Div}\, \mathbb{D} = 0, \quad \text{Curl}\, \mathbb{E} = \mathbb{0} \quad \text{in } \mathcal{B}_0. \tag{7}$$

The expressions Div and Curl are the corresponding differential operators defined with respect to the material position vector $\boldsymbol{X}$. The second Maxwell equation is fulfilled a priori when the electric field $\mathbb{E}$ is derived from a scalar electric potential ϕ, i.e.

$$\mathbb{E} = -\text{Grad}\, \phi, \quad \text{in } \mathcal{B}_0. \tag{8}$$

In electro-mechanics the balance of linear momentum takes the form

$$\text{Div}\, \boldsymbol{P}^{\text{tot}} + \boldsymbol{b}_0 = \boldsymbol{0} \quad \text{in } \mathcal{B}_0, \tag{9}$$

with the total Piola stress tensor $\boldsymbol{P}^{\text{tot}}$, which can be decomposed into a purely mechanical contribution $\boldsymbol{P}$ and a ponderomotive contribution $\boldsymbol{P}^{\text{pon}}$. The latter stress contains the polarization stress $\boldsymbol{P}^{\text{pol}}$ and the Maxwell stress $\boldsymbol{P}^{\text{max}}$ [33]. We complete our description with the formulation of the necessary jump conditions describing the behavior of the electric and mechanical problem at a possible surface of discontinuity. When we denote the jump of a quantity between both sides of the discontinuity as

$[\![\bullet]\!]$, the formulation reads

$$[\![\mathbb{D}]\!] \cdot \boldsymbol{N} = \hat{\varrho}_0^f, \quad \text{on } \partial\mathcal{B}_0^\varrho \quad \text{and} \quad -[\![\boldsymbol{P}^{\text{tot}}]\!] \cdot \boldsymbol{N} = \boldsymbol{t}_0^p, \quad \text{on } \partial\mathcal{B}_0^t, \tag{10}$$

where $\boldsymbol{N}$ is the outwards pointing surface normal, $\boldsymbol{t}_0^p$ are the mechanical tractions prescribed on the part of the boundary $\partial\mathcal{B}_0^t$ and $\hat{\varrho}_0^f$ is the density of free surface charges per undeformed area on the part of the boundary $\partial\mathcal{B}_0^\varrho$ [34, 35].

2.3 Constitutive equations

As a starting point for the derivation of constitutive equations, we use the local form of the balance of energy in the material configuration. For the quasi static case this reads

$$\dot{\mathcal{U}} = \boldsymbol{P} : \dot{\boldsymbol{F}} - \text{Div}\, \boldsymbol{Q} + \mathcal{R} + \mathbb{E} \cdot \dot{\mathbb{P}} + \boldsymbol{P}^{\text{pol}} : \dot{\boldsymbol{F}}. \tag{11}$$

Here, we introduce the change in the internal energy density per unit undeformed volume $\dot{\mathcal{U}}$, the heat source $\mathcal{R}$ and the heat flux vector $\boldsymbol{Q}$, which can be calculated from the gradient of the absolute temperature Θ using the Fourier type relation $\boldsymbol{Q} := -\kappa_{\text{con}} J \boldsymbol{C}^{-1} \cdot \text{Grad}\, \Theta$, where κ_{con} is the isotropic heat conductivity. Next the dissipation power density $\mathcal{D} = \mathcal{D}(\boldsymbol{X}, t) \geq 0$ is introduced that can be decomposed into the dissipation power density due to the heat conduction $\mathcal{D}^{\text{con}} = -\dfrac{\boldsymbol{Q}}{\Theta} \cdot \text{Grad}\, \Theta \geq 0$ and the local dissipation power density $\mathcal{D}^{\text{loc}}$ [36], which can be defined in the form of the Clausius-Planck inequality as

$$\mathcal{D}^{\text{loc}} = \Theta \dot{H} - \dot{\mathcal{U}} + \boldsymbol{P} : \dot{\boldsymbol{F}} + \mathbb{E} \cdot \dot{\mathbb{P}} + \boldsymbol{P}^{\text{pol}} : \dot{\boldsymbol{F}} \geq 0, \tag{12}$$

using the entropy density H. It should be noted that in the case of a reversible process, the local dissipation term vanishes. With the help of a Legendre transformation [37], a formulation for the energy density $\Psi(\boldsymbol{F}, \Theta, \mathbb{E})$ can be obtained as

$$\Psi(\boldsymbol{F}, \Theta, \mathbb{E}) = \mathcal{U} - \Theta H - \mathbb{E} \cdot \mathbb{P}. \tag{13}$$

Using this energy density, the Clausius-Planck inequality can be transformed to

$$\mathcal{D}^{\text{loc}} = -\dot{\Psi} - \dot{\Theta} H + [\boldsymbol{P} + \boldsymbol{P}^{\text{pol}}] : \dot{\boldsymbol{F}} - \dot{\mathbb{E}} \cdot \mathbb{P} \geq 0. \tag{14}$$

Note that in the formulation of $\Psi(\boldsymbol{F}, \Theta, \mathbb{E})$ the energy that is stored in the electric field itself is not taken into account. In order to consider this energy contribution as well, we have to amend the energy density by the term $E(\boldsymbol{F}, \mathbb{E}) = -\frac{1}{2} \varepsilon_0 J [\mathbb{E} \otimes \mathbb{E}] : \boldsymbol{C}^{-1}$, which leads to the amended total energy density per unit volume in $\mathcal{B}_0$ [38, 39]

$$\Omega(\boldsymbol{F}, \Theta, \mathbb{E}) = \Psi(\boldsymbol{F}, \Theta, \mathbb{E}) + E(\boldsymbol{F}, \mathbb{E}). \tag{15}$$

When the amended energy function $\Omega(\boldsymbol{F}, \Theta, \mathbb{E})$ is inserted into the Clausius-Planck inequality we find a formulation that contains the total Piola stress and the electric displacement

$$\mathcal{D}^{\text{loc}} = -\dot{\Omega} - \dot{\Theta} H + \boldsymbol{P}^{\text{tot}} : \dot{\boldsymbol{F}} - \dot{\mathbb{E}} \cdot \mathbb{D} \geq 0, \tag{16}$$

which further establishes the constitutive relations for the total Piola stress $\boldsymbol{P}^{\text{tot}}$, the electric displacement $\mathbb{D}$ and the entropy H [33]

$$\boldsymbol{P}^{\text{tot}} = \frac{\partial \Omega}{\partial \boldsymbol{F}}, \quad \text{with} \quad \boldsymbol{P}^{\max} = \frac{\partial E}{\partial \boldsymbol{F}}, \quad \mathbb{D} = -\frac{\partial \Omega}{\partial \mathbb{E}}, \quad H = -\frac{\partial \Omega}{\partial \Theta}. \tag{17}$$

It is convenient to introduce the total Piola-Kirchhoff stress $\boldsymbol{S}^{\text{tot}}$ as an additional stress measure, which is related to the Piola stress by $\boldsymbol{S}^{\text{tot}} = \boldsymbol{F}^{-1}\boldsymbol{P}^{\text{tot}}$. As presented in Appendix 6.1, the introduced intermediate configuration $\mathcal{B}_{EM}$ can be used to define a corresponding form $\boldsymbol{S}^{\text{tot}}_{EM}$ of the Piola-Kirchhoff stress that is connected to $\boldsymbol{S}^{\text{tot}}$ via

$$\boldsymbol{S}^{\text{tot}} = \boldsymbol{F}^{-1}_{EM} \cdot \boldsymbol{S}^{\text{tot}}_{EM} \cdot \boldsymbol{F}^{-T}_{EM}. \tag{18}$$

This enables us to use an energy function that does not explicitly contain a contribution connected to the thermal expansion through the expression

$$\boldsymbol{S}^{\text{tot}} = 2J_{\Theta}^{-\frac{2}{3}} \frac{\partial \Omega(\boldsymbol{F}_{EM}, \Theta, \mathbb{E})}{\partial \boldsymbol{C}_{EM}}. \tag{19}$$

Finally, the first law of thermodynamics in entropy form is derived by combining the Clausius-Planck inequality (14) with (11), resulting in

$$c(\Theta)\dot{\Theta} = \mathcal{R} - \text{Div}\boldsymbol{Q} + \underbrace{\Theta \partial_{\Theta}\left[\boldsymbol{P}^{\text{tot}} : \dot{\boldsymbol{F}} - \mathbb{D} \cdot \dot{\mathbb{E}}\right]}_{\mathcal{H}} + \mathcal{D}^{\text{loc}}, \tag{20}$$

where the specific heat capacity $c(\Theta)$ at constant deformation and constant electric field is introduced. The terms in brackets on the right-hand side of the above equation describe possible heating/cooling effects due to mechanical deformation, i.e. the Gough-Joule effect, or the application of an electric field. These are summarized in the term $\mathcal{H}$ in order to tighten the expression. We can finalize the thermal description of our system by imposing boundary conditions for the thermal system in addition to the ones for the mechanical and the electric problem defined earlier. We impose Dirichlet boundary conditions for the temperature and Neumann boundary conditions for the heat flux on the boundary $\partial\mathcal{B}_0 = \partial\mathcal{B}_0^{\Theta} \bigcup \partial\mathcal{B}_0^{Q}$.

$$\Theta = \Theta^{p} \quad \text{on } \partial\mathcal{B}_0^{\Theta} \quad \text{and} \quad \boldsymbol{Q} \cdot \boldsymbol{N} = \overline{Q} \quad \text{on } \partial\mathcal{B}_0^{Q}. \tag{21}$$

3 A thermo-electro-viscoelastic constitutive model

In the following, the constitutive modeling approach for the description of the material response of VHB 4905$^{\text{TM}}$ under combined thermo-electro-mechanical loading is described in detail. It is assumed that the underlying material can be characterized as isotropic. Thus, the material response to an electro-mechanical loading can be expressed using a function of the six principal invariants I_1 to I_6 connected to the electro-mechanical right Cauchy-Green tensor $\boldsymbol{C}_{EM}$ and the electric field $\mathbb{E}$, which read

$$\begin{aligned} &I_1 = \text{tr}\,(\mathbf{C}_{EM}), \quad I_2 = \frac{1}{2}\Big[[\text{tr}\,(\mathbf{C}_{EM})]^2 - \text{tr}\,(\mathbf{C}_{EM}{}^2)\Big], \quad I_3 = \det\,(\mathbf{C}_{EM}), \\ &I_5 = [\mathbb{E}\otimes\mathbb{E}] : \mathbf{C}_{EM}, \quad I_6 = [\mathbb{E}\otimes\mathbb{E}] : \mathbf{C}_{EM}^2. \end{aligned} \tag{22}$$

In order to capture the thermal loading, a temperature-dependent form of the energy function has to be derived. When we assume that the temperature may in general have a nonlinear effect on the material response, such a coupling may be established starting with the definition of the specific heat capacity c at constant deformation and electric field, i.e.

$$c|_{\boldsymbol{F},\mathbb{E}}(\Theta) = c_0 - \Theta\frac{\partial^2 g(\Theta)}{\partial\Theta^2}\widetilde{\Psi}_0(\mathbf{C}_{EM},\mathbb{E}). \tag{23}$$

Here, we have introduced a constant ground heat capacity c_0 and the scaling function $g(\Theta)$ that is connected multiplicatively with the energy function $\widetilde{\Psi}_0$, which describes the response of the material at the reference temperature. This approach renders the thermally coupled energy function as

$$\Psi = f(\Theta)\widetilde{\Psi}_0(\mathbf{C}_{EM},\mathbb{E}) + \mathcal{U}_0\left[1 - \frac{\Theta}{\Theta_0}\right] + c_0\left[\Theta - \Theta_0 - \Theta\ln\left(\frac{\Theta}{\Theta_0}\right)\right], \tag{24}$$

where we have introduced the internal energy at reference temperature $\mathcal{U}_0$ and a thermal scaling function of the energy that is defined as

$$f(\Theta) = \frac{\Theta}{\Theta_0} + g(\Theta) - g(\Theta_0) + \left.\frac{\partial g(\Theta)}{\partial\Theta}\right|_{\Theta_0}[\Theta - \Theta_0]. \tag{25}$$

A detailed derivation of this expression is given in Appendix 7. For the sake of readability, the index of the isothermal energy contribution $\widetilde{\Psi}_0$ is discarded in the following and the respective term is simply labeled as $\widetilde{\Psi}$. In order to correctly replicate the highly viscous material response of electro-active polymers such as VHB 4905$^{\text{TM}}$, the energy contribution $\widetilde{\Psi}(\boldsymbol{C}_{EM},\mathbb{E})$ has to be modified into the form $\widetilde{\Psi}(\boldsymbol{C}_{EM},\mathbb{E},\boldsymbol{A}_i)$ that, in addition to the non-thermal deformation and the electric field, also depends on strain-like internal variables $\boldsymbol{A}_i$. These tensorial variables correspond to a number of Maxwell elements that capture a time dependency of the material response. We assume that the energy $\widetilde{\Psi}(\boldsymbol{C}_{EM},\mathbb{E},\boldsymbol{A}_i)$ can be decomposed

into a contribution $\widetilde{\Psi}_{\text{vol}}(J_{\text{EM}})$ that represents the volumetric change of the material due to electro-mechanical deformation, and a volume preserving contribution $\widetilde{\Psi}_{\text{iso}}\left(\overline{\boldsymbol{C}}_{\text{EM}}, \mathbb{E}, \boldsymbol{A}_i\right)$, the first of which vanishes, when the material is considered to be incompressible at constant temperature. The latter term depends on the modified right Cauchy-Green tensor $\overline{\boldsymbol{C}}_{EM} = J_{EM}^{-2/3}\boldsymbol{C}_{EM}$ and can be further decomposed into an elastic part $\widetilde{\Psi}^{e}_{\text{iso}}\left(\overline{\boldsymbol{C}}_{\text{EM}}, \mathbb{E}\right)$ and a viscous contribution $\widetilde{\Psi}^{v}_{\text{iso}}\left(\overline{\boldsymbol{C}}_{\text{EM}}, \mathbb{E}, \boldsymbol{A}_i\right)$. Based on the thermo-mechanical experimental results in Part I, we can assume that, in order to replicate the effect of temperature on the material response, both the elastic and the viscous energy contributions have to be modified by a respective scaling function. Consequently, the term $f(\Theta)$, introduced in equation (25), expands to the expressions $f^e(\Theta)$ and $f^v(\Theta)$ as separate scaling functions, which are multiplied with the respective energy contribution. Thus, as presented in [40], the heat capacity takes the form

$$c(\Theta) = c_0 - \Theta\frac{\partial^2 g^e(\Theta)}{\partial\Theta^2}\widetilde{\Psi}^{e}_{\text{iso}}\left(\overline{\boldsymbol{C}}_{\text{EM}}, \mathbb{E}\right) - \Theta\frac{\partial^2 g^v(\Theta)}{\partial\Theta^2}\widetilde{\Psi}^{v}_{\text{iso}}\left(\overline{\boldsymbol{C}}_{\text{EM}}, \mathbb{E}, \boldsymbol{A}_i\right). \tag{26}$$

The energy function is formulated on the intermediate configuration $\mathcal{B}_{EM}$. Therefore, the internal energy contribution describing the thermal expansion of the material is not included explicitly, resulting in an expression for the thermo-electro-viscoelastic energy function that reads

$$\Psi(\boldsymbol{F}_{EM}, \mathbb{E}, \Theta) = f^e(\Theta)\widetilde{\Psi}^{e}_{\text{iso}}\left(\overline{\boldsymbol{C}}_{\text{EM}}, \mathbb{E}\right) + f^v(\Theta)\widetilde{\Psi}^{v}_{\text{iso}}\left(\overline{\boldsymbol{C}}_{\text{EM}}, \mathbb{E}, \boldsymbol{A}_i\right) - c_0 k(\Theta), \tag{27}$$

where the term $\left[\Theta - \Theta_0 - \Theta\ln\left(\frac{\Theta}{\Theta_0}\right)\right]$ is summarized as $k(\Theta)$ for the sake of brevity.

3.1 Electro-viscoelastic modeling approach

Following the structure of the experimental investigations presented in Part I, we begin by specifying the zero field elastic part of the energy function. Based on the information from the multi-step relaxation tests performed at room temperature and the equilibrium values for the resulting force we select a Yeoh-type energy function [41] for the representation of the zero field base elasticity, i.e.,

$$\widetilde{\Psi}^{e}_{\text{iso}}(\overline{\boldsymbol{C}}_{\text{EM}}) = c_1\left[\overline{I}_1 - \dim\right] + c_2\left[\overline{I}_1 - \dim\right]^2 + c_3\left[\overline{I}_1 - \dim\right]^3. \tag{28}$$

This model is derived from the class of Mooney-Rivlin models [42] but does not consider the second invariant. Thus, it is exclusively based on the first invariant of the modified right Cauchy-Green tensor $\overline{I}_1 = \text{tr}\left(\overline{\boldsymbol{C}}_{\text{EM}}\right)$ up to power three, with three material parameters c_1, c_2 and c_3. These parameters will be identified using the results of the multi-step relaxation experiments performed at room temperature. In the context of the current work, the function is formulated independently from the dimension of the space under consideration. Therefore, Equation (28) contains the

expression "dim" that refers to the currently considered dimension. In the case of the experiments, the value of "dim" is set to 3.
It should be noted that this choice differs from the one made in [43], where the micromechanically motivated eight-chain model was selected. As our experiments on VHB are restricted to a range of a maximum stretch of 200%, the material stress-strain behavior does not show a particularly complex non-linear response. Thus, the identified material parameters presented in [43] transform the selected eight-chain model into a form that is reduced to a simple polynomial type energy function, rendering the complexity of the selected micro-mechanically motivated approach redundant. Consequently, in the context of this work, the Yeoh-type energy function is selected as a more straight-forward approach.
Next, the viscous response (mechanical) of the material is modelled by specifying $\widetilde{\Psi}^{v}_{\text{iso}}\big(\overline{\boldsymbol{C}}_{\text{EM}}, \boldsymbol{A}_i\big)$. As the resulting curves in the cyclic loading tests do not show a distinctive S-shape, the viscous energy contribution takes the form of a Neo-Hookean type formulation with the respective evolution law defined for the strain-like internal variables $\boldsymbol{A}_i$ [44], i.e.,

$$\widetilde{\Psi}^{v}_{\text{iso}}(\overline{\boldsymbol{C}}_{\text{EM}}, \boldsymbol{A}_i) = \sum_{i=1}^{3} \frac{\mu_i^v}{2}\left[\overline{I}^{v}_{1,i} - \text{dim}\right], \text{where } \dot{\boldsymbol{A}}_i \quad = \frac{1}{\tau_i}\left[\overline{\boldsymbol{C}}_{\text{EM}} - \frac{1}{\text{dim}}\overline{I}^{v}_{1,i}\boldsymbol{A}_i\right]. \quad (29)$$

Note that in the above formulation, we define the term $\overline{I}^{v}_{1,i} = \boldsymbol{A}_i^{-1} : \overline{\boldsymbol{C}}_{\text{EM}}$. In these definitions, the viscous shear moduli μ_i^v and the relaxation times τ_i have been introduced. In accordance with our previous works [45, 46], we select three internal variables. Thus, three pairs of shear moduli and relaxation times have to be identified using the results of the cyclic loading tests conducted at room temperature.
In order to replicate the effect of temperature on the material, the scaling functions $g^e(\Theta)$ and $g^v(\Theta)$ have to be specified. It should be noted that due to the restrictions of the available testing equipment and real life application scenarios of VHB, the temperatures that are considered in the context of this work are restricted to a range from room temperature up to 60°C. Thus, the temperature scaling functions do not need to have the potential to reflect the more complex effects around the glass transition temperature that, according to the VHB 4905$^{\text{TM}}$ performance manual supplied by 3M$^{\text{TM}}$, is at −40°C [47]. The elastic scaling function $g^e(\Theta)$ is therefore defined as a simple quadratic relation in terms of the temperature change $\Delta\Theta = \Theta - \Theta_0$, i.e.

$$g^e(\Theta) = \left[-\frac{\Theta}{\Theta_0} + 1 - a_1^e\Delta\Theta - a_2^e\Delta\Theta^2\right]. \quad (30)$$

Here, we have introduced two additional material parameters a_1^e and a_2^e that have to be identified using the results of the multi-step relaxation experiments performed at different temperatures. For the viscous scaling function $g^v(\Theta)$, a formulation from [48, 40] is adapted that reads

$$g^v(\Theta) = \left[-\frac{\Theta}{\Theta_0} + \exp\left(a^v\left[1 - \frac{\Theta}{\Theta_0}\right]\right)\right], \quad (31)$$

where the additional material parameter a^v is introduced that has to be identified using the cyclic loading tests performed at increased temperatures.
Finally, the coupling of the mechanical material response to the application of an electric field has to be established. For this, numerous different formulations can be found in the literature, amongst others in the publications of Ask et al. [17, 49], Saxena et al. [50] or Jabareen [51]. The approach adopted in the context of this work originates from the ideas presented in the works of Steinmann [52] and Dorfmann and Ogden [53]. Generally we assume that the influence of the free space, surrounding the material may be neglected due to the capacitor like characteristics of the applications under consideration [52]. The electro-mechanical coupling is established by additional terms in the energy function, one of which is depending on the fifth invariant $I_5 = [\mathbb{E} \otimes \mathbb{E}] : \mathbf{C}$, defined in Equation (59). Thus, similar to the formulation given in [52], the coupled form of the isothermal energy contribution $\widetilde{\Psi}^e_{\text{iso}} = \widetilde{\Psi}^e_{\text{iso}}(\overline{\boldsymbol{C}}_{\text{EM}}, \mathbb{E})$ reads

$$\widetilde{\Psi}^e_{\text{iso}}(\overline{\boldsymbol{C}}_{\text{EM}}, \mathbb{E}) = c_1\left[\overline{I}_1 - \text{dim}\right] + c_2\left[\overline{I}_1 - \text{dim}\right]^2 + c_3\left[\overline{I}_1 - \text{dim}\right]^3 + \gamma_1 I_4 + \gamma_2 I_5. \quad (32)$$

The reader should note that the expression $\gamma_1 I_4$ characterizes the purely electric behavior of the material and can therefore not be identified using the presented experiments. However, as it does not influence the mechanical response of the material, it will not be investigated in the scope of this work.
The formulation is extended by the idea presented in [53] that the mechanical material parameters may be dependent on the electric field. In the case of the Yeoh-type energy function, we choose to incorporate a dependency of c_1 on the electric field in the form $c_1 := c_1(I_4) = \hat{c}_1 - \beta^e I_4$. This relation conveys the notion that the material has a ground state elasticity described by the parameter $\hat{c}_1$ that is influenced by the application of an electric field, scaled by the coupling parameter β^e. Alternatively, the parameter $c_1(\mathbb{E})$ is also multiplied with the purely mechanical first invariant I_1, which may be interpreted as a deformation-dependent formulation of the coupling parameters. Thus, the approach chosen herein is in accordance with the concepts presented in [49, 51]. Within the scope of this work, we will extend on the formulation given in [40], in which the field sensitivity is captured exclusively by additional terms in the elastic energy contribution. Furthermore, a dependency of the viscous material parameters on the electric field is also assumed similar to the form presented in [40].Thus the viscous shear moduli from Equation (29) are defined as $\mu^v_i := \mu^v_i(I_4) = \hat{\mu}^v_i - \beta^v_i I_4$ with the ground state viscous shear moduli $\hat{\mu}^v_i$ and the coupling parameters β^v_i. In order to ease the orientation among the numerous introduced material parameters, the required quantities are summarized in Table 3.1.

4 Parameter identification

Using the experimental results presented in Part I, all material parameters appearing in the constitutive model as introduced in the previous section can be identified.

Mechanical Base Parameters								
Elastic Parameters			Viscous Parameters					
c_1	c_2	c_3	$\hat{\mu}_1^v$	$\hat{\mu}_2^v$	$\hat{\mu}_3^v$	τ_1	τ_2	τ_3
Coupling Parameters								
Thermal Scaling Parameters			Electro-Mechanical Coupling Parameters					
a_1^e	a_2^e	a^v	β^e	γ_2	β_1^v	β_2^v	β_3^v	

To this end, the same approach as presented in [43, 47] is adopted here. Thus, analytical solutions that correspond to the purely mechanical and thermo-mechanical experiments have to be derived. Based on the selected sample dimensions during the experiments, the stress state can be assumed to be one-dimensional. Moreover, when we consider the material to be incompressible at constant temperature, the resulting deformation gradient and the corresponding right Cauchy-Green tensor in the intermediate configuration, formulated in terms of the applied strain λ, take the form

$$\boldsymbol{F}_{EM} = \begin{bmatrix} \lambda & 0 & 0 \\ 0 & \lambda^{-1/2} & 0 \\ 0 & 0 & \lambda^{-1/2} \end{bmatrix}, \quad \boldsymbol{C}_{EM} = \begin{bmatrix} \lambda^2 & 0 & 0 \\ 0 & \lambda^{-1} & 0 \\ 0 & 0 & \lambda^{-1} \end{bmatrix}. \tag{33}$$

Therefore, the strain-like internal variables $\boldsymbol{A}_i$ take a form, resembling $\boldsymbol{C}_{EM}$, i.e.

$$\boldsymbol{A}_i = \begin{bmatrix} A_i^2 & 0 & 0 \\ 0 & A_i^{-1} & 0 \\ 0 & 0 & A_i^{-1} \end{bmatrix}. \tag{34}$$

With the above definitions at hand, the corresponding Piola stresses can be derived. For the sake of simplicity, we begin with the purely mechanical case, i.e., the resulting stress contributions at reference temperature without the application of an electric field. Using the expressions for the elastic (28) and the viscous energy contribution $(29)_1$, these stresses take the form

$$\begin{aligned} P^e_{\text{iso}} &= \frac{4}{3}\left[c_1 + 2c_2\left[\lambda^2 + 2\lambda^{-1} - \dim\right] + 3c_3\left[\lambda^2 + 2\lambda^{-1} - \dim\right]^2\right]\left[\lambda - \lambda^{-2}\right], \\ P^v_{\text{iso,i}} &= \frac{4}{3}\mu_i^v\left[\lambda A_i^{-2} - \lambda^{-2} A_i\right]. \end{aligned} \tag{35}$$

The internal variables A_i can be obtained from the evolution law $(29)_2$ by using an implicit Euler integration method combined with a Newton-type iterative scheme. Now the material parameters can be identified by fitting the expression for the Piola stress to the experimental results. This identification begins with the elastic parameters c_i of the Yeoh-type model. As it is assumed that the equilibrium values correspond to the purely elastic response of the material, the elastic material parameters are identified by minimizing the objective function

$$\frac{[P^e_{\text{iso}}]A - F^n_{\text{exp}}}{F_{\text{exp}}}. \tag{36}$$

Here the undeformed cross section A and the experimental values of the applied force F_{exp} are introduced. The optimal solution is found using the nonlinear least-squares solver *lsqnonlin* in Matlab, resulting in a fit of the analytical solution (dashed line) to the experimental results (solid line) as depicted in Figure 2 with the values for the material parameters $c_1 = 1.603 \cdot 10^{-2}\text{N/mm}^2$, $c_2 = -8.1407 \cdot 10^{-4}\text{N/mm}^2$ and $c_3 = 4.6951 \cdot 10^{-5}\text{N/mm}^2$.

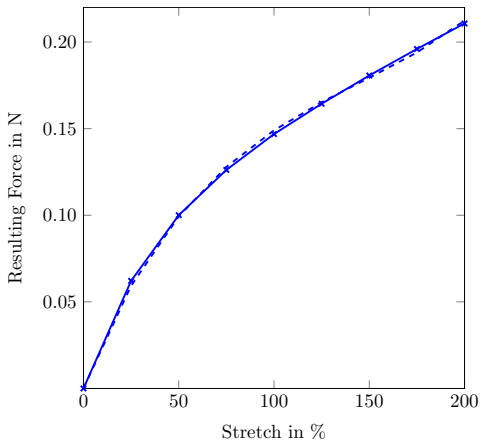

Fig. 2 Analytical solution (dashed line) is fitted to the experimental results (solid line), in which the equilibrium values are obtained from a multi-step relaxation test that is performed at constant reference temperature.

It is clearly visible that the model for the elastic response of the material results in an excellent replication of the experimental results. It should be emphasized again that the stress-strain curve of VHB does not show the S-shape, which is a characteristic for most polymeric materials. This is because the maximum applied deformation applied in our experiments is not in the range in which the strain hardening occurs. However, the selected Yeoh-type material model is in general capable of reproducing such hardening due to its cubic formulation as shown in [42]. In order to quantify the quality of the fit, the coefficient of determination R^2 can be introduced as

$$R^2 = 1 - \frac{\sum_{i=1}^{n}[y_i - \hat{y}_i]^2}{\sum_{i=1}^{n}[y_i - \overline{y}]^2}. \tag{37}$$

Here, the difference between the experimental results y_i and the simulation $\hat{y}_i$ are normalized by the difference between the experimental results and their average value $\overline{y}$ [46], thus R^2 can take a value between 1, corresponding to a perfect fit between the model and the experiment, and 0. For Figure 2 the coefficient of determination is 0.9993.

Once the elastic parameters are identified, the viscous material parameters, namely μ_i^v and τ_i, can be identified by fitting the analytical solution to the experimental results of the cyclic loading tests. The identification could be performed using the data of a cyclic loading test at one specific strain rate. However, as we consider a number of three internal variables, the values for the three parameter pairs are not unique. This means, when we identify a set of material parameters with the help of the data of only one strain rate, the identified parameters do not necessarily fit the curves of the other strain rates. Thus, a *simultaneous minimization* technique [54, 55, 56] is adopted to identify a unique set of material parameters that can work for data with all specified strain rates under consideration. To this end, for the values of the viscous material parameters, an optimization objective reads

$$\sum_{n=1}^{s} \frac{\left[P_{\text{iso}}^{e,n} + P_{\text{iso}}^{v,n}\right] A - F_{\text{exp}}^{n}}{F_{\text{exp}}^{n}}, \tag{38}$$

where s is the number of strain rates taken into account for the optimization routine. As in the elastic case, this problem is solved using the *lsqnonlin* optimization function integrated within Matlab. The results of the strain rates $\dot{\lambda} = [0.025\ \text{s}^{-1}, 0.1\ \text{s}^{-1}, 0.2\ \text{s}^{-1}]$ are used for the optimization, while the remaining data from $\dot{\lambda} = 0.05\,\text{s}^{-1}$ is used for additional validation of the identified parameters. Table 1 shows the identified values for the parameter sets.

μ_1^v	μ_2^v	μ_3^v	τ_1	τ_2	τ_3
$5.76 \cdot 10^{-2}$	$1.47 \cdot 10^{-2}$	$9.01 \cdot 10^{-3}$	0.81	27.35	763.67

Table 1 Identified material parameter sets. μ_i^v in N/mm^2 and τ_i in s.

Figure 3 depicts a comparison between the analytically obtained results (dashed lines) and the respective experimental results.

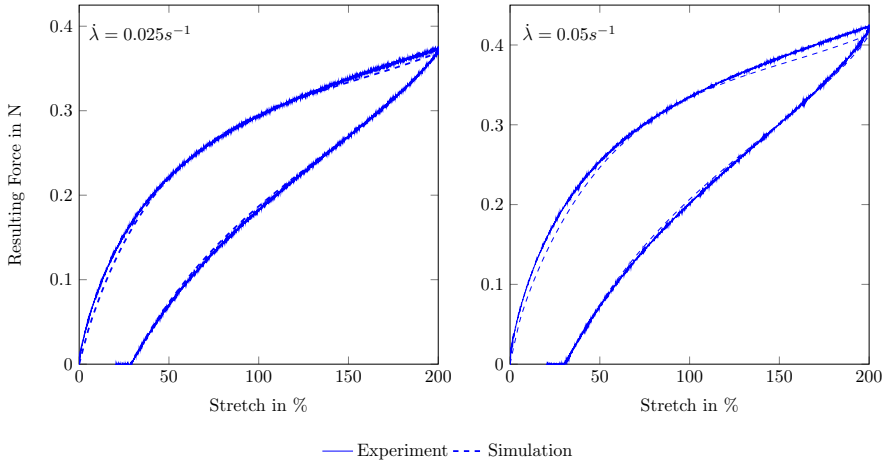

(a) Loading-unloading test with $\dot{\lambda}$ = 0.025 s^{-1} and $\dot{\lambda}$ = 0.05 s^{-1}

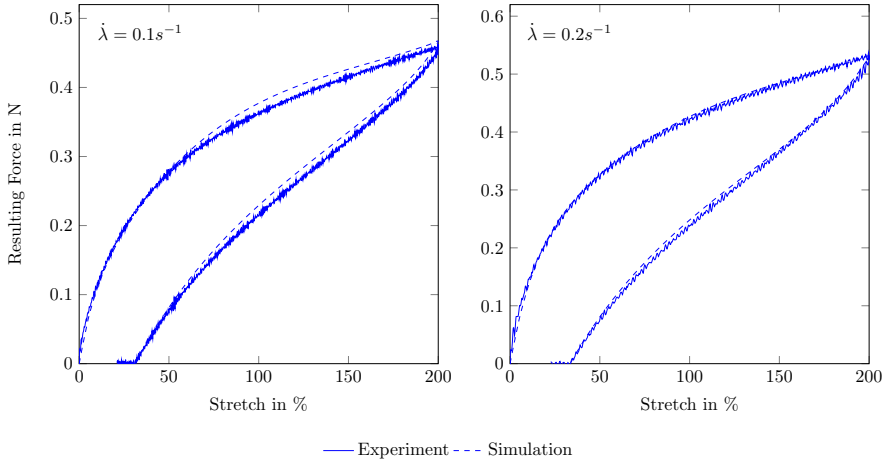

(b) Loading-unloading test with $\dot{\lambda}$ = 0.1 s^{-1} and $\dot{\lambda}$ = 0.2 s^{-1}

Fig. 3 Comparison between the experimental results (solid lines) and the simulation (dashed lines) results for cyclic loading tests performed at various strain rates at reference temperature.

The plots show that the model is able to replicate the material response satisfyingly well both for the strain rates that are used for the parameter identification as well as for the remaining validation data. For the former, the coefficient of determination ranges from 0.9982 to 0.9964 and for the latter the value is 0.9942. As an additional validation, the results of the multi-step relaxation test can also be replicated. In Figure 4, a comparison between the experimental results and the simulation results is depicted.

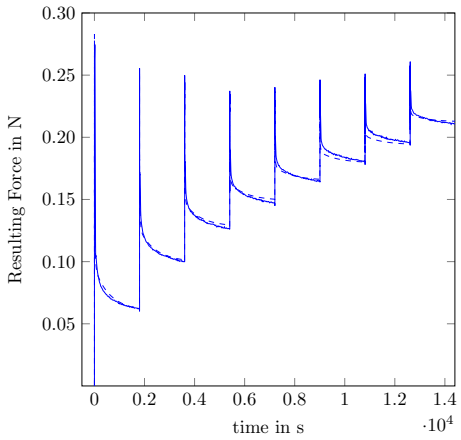

Fig. 4 Comparison between the simulation results (dashed line) and the experimental data (solid line) that are obtained from a multi-step relaxation test performed at reference temperature.

Note that during the entire course of the multi-step relaxation test, the selected material model, in combination with the identified material parameters, is capable of replicating the material response with an excellent agreement. This holds true when the material response is dominated by viscous effects, i.e., the initial peak followed by the subsequent relaxation behavior of the applied force, and the final equilibrium phase of each step, where the response is dominated by the elastic contribution.
Now, the identified purely mechanical parameters will enable us to utilize the results of the experiments conducted at increased temperatures for the identification of the thermo-coupling parameters. For this, the same approach is adopted as in the purely mechanical case. However, the calculated stresses now contain the respective scaling functions $f(\Theta)^e$ and $f(\Theta)^v$ related to $g^e(\Theta) = \left[-\frac{\Theta}{\Theta_0} + 1 - a_1^e \Delta\Theta - a_2^e \Delta\Theta^2\right]$ and $g^v(\Theta) = \left[-\frac{\Theta}{\Theta_0} + \exp(a^v[1 - \frac{\Theta}{\Theta_0}])\right]$, thus rendering the temperature sensitive stresses in the format

$$\begin{aligned} \widetilde{P}^e_{\text{iso}} &= \left[1 - \left[\frac{1}{\Theta_0} + 2a_1^e\right]\Delta\Theta - a_2^e \Delta\Theta^2\right] J_\Theta^{-\frac{2}{3}} P^e_{\text{iso}}, \\ \widetilde{P}^v_{\text{iso,i}} &= \left[\exp\left(a^v\left[1 - \frac{\Theta}{\Theta_0}\right]\right) + [1 + a^v]\left[1 - \frac{\Theta}{\Theta_0}\right]\right] J_\Theta^{-\frac{2}{3}} P^v_{\text{iso,i}}. \end{aligned} \tag{39}$$

In this context, the terms P^e_{iso} and $P^v_{\text{iso,i}}$ refer to the respective stresses at reference temperature given in Equation (35) and J_Θ is the determinant of the thermal deformation gradient. Using the results from the multi-step relaxation experiments conducted at various temperatures, the parameters a_1^e and a_2^e of the elastic scaling function can be identified. Figure 5 shows the results of the fitting procedure, in which the values of the parameters $a_1^e = 4.015 \cdot 10^{-3} K^{-1}$ and $a_2^e = -1.349 \cdot 10^{-4} K^{-2}$ are identified.

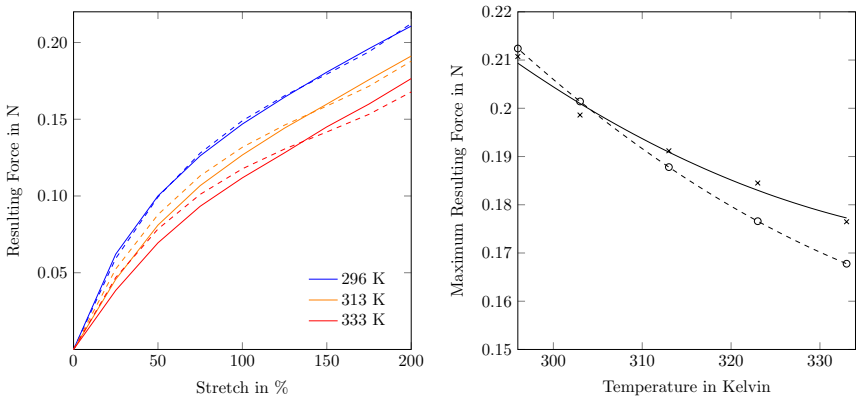

Fig. 5 Simulation results meet with experimental data. The equilibrium values are extracted from the relaxed points of the multi-step relaxation tests performed at different temperatures. (Left) Simulation (dashed lines) and experimental values (solid lines) over the applied stretch. (Right) Simulation (o-marks and dashed trend line) and experimental values (x-marks and solid line) of the resulting force for the maximum applied stretch over the temperature range.

Figure 5 shows that for the narrow temperature range under consideration, the simple form of the scaling function $g^e(\Theta)$ is sufficient to replicate the effect of the temperature on the elastic material response satisfyingly well. Thus, we can proceed with the identification of the material parameter c of the viscous coupling function. For the identification, the experimental results of the cyclic loading tests at 0.1 s^{-1} performed under the temperatures 40°C and 60°C are used. Therefore, the data obtained from the experiments conducted at a strain rate of 0.1 s^{-1} at the temperatures of 30°C and 50°C and the entire data from the remaining strain rates can be used for the validation. Figures 6 to 9 show a comparison between the simulation results and the experiments with an identified value of the thermo-coupling parameter $a^v = 1.7934$.

The results depicted in Figures 6 to 9 indicate that the choice of the viscous scaling function $g^v(\Theta)$ leads to an excellent fit of the cyclic loading experiments for all of the strain rates and temperatures under consideration.
Finally, on the basis of the identified purely mechanical parameters, the values of the electro-mechanical coupling parameters can be found using an approach similar to the one from the previous sections. However, due to the selected sample geometry and the boundary conditions of the electro-mechanical experiments, the resulting deformation can not be considered as a uniaxial stress state. Therefore, the problem can not be solved analytically and the finite element implementation described in [40, 46] has to be used to mimic the experiments. The data from the electro-mechanical experiments at the maximum applied voltage of 6 kV at three different

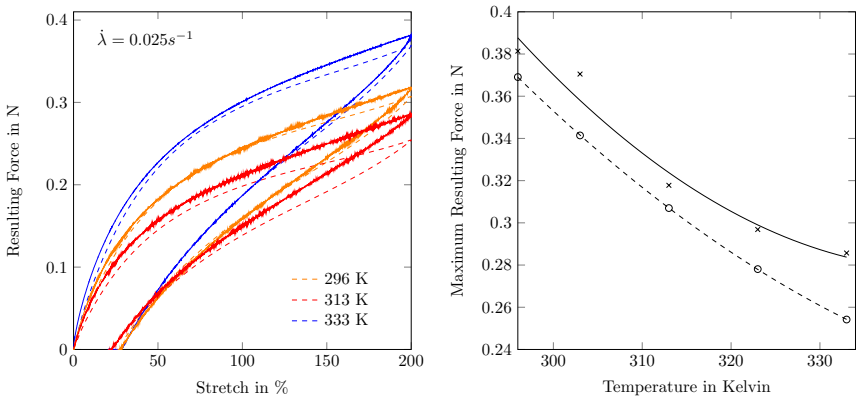

Fig. 6 Simulation results are compared with experimental data that are obtained from the cyclic loading tests conducted at different temperatures. (Left) Simulation (dashed lines) and experimental values (marks) over the applied stretch. (Right) Simulation (o-marks and dashed trend line) and experimental values (x-marks and solid line) of the resulting force for the maximum applied stretch over the temperature range for the strain rate of 0.025 s^{-1}.

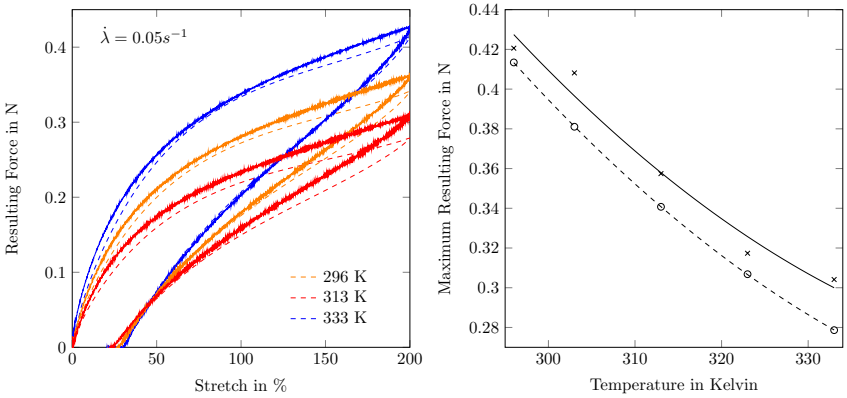

Fig. 7 Simulations compared to experiments for the values of the resulting force of cyclic loading tests at different temperatures. (Left) Simulation (dashed lines) and experimental values (marks) over the applied stretch. (Right) Simulation (o-marks and dashed trend line) and experimental values (x-marks and solid line) of the resulting force for the maximum applied stretch over the temperature range for the strain rate of 0.05 s^{-1}.

strain rates is used for the optimization. Furthermore, the results from the remaining electro-mechanical experiments conducted with 2 kV - 5 kV for all strain rates can be used as the validation of the model with the identified parameters. This simultaneous optimization routine makes the use of the same optimization function as previously introduced in Equation (38). Therein, the calculated stress values are obtained from the finite element computation. The amount of experimental data that is chosen for the optimization routine is small compared to the remaining validation data. This is

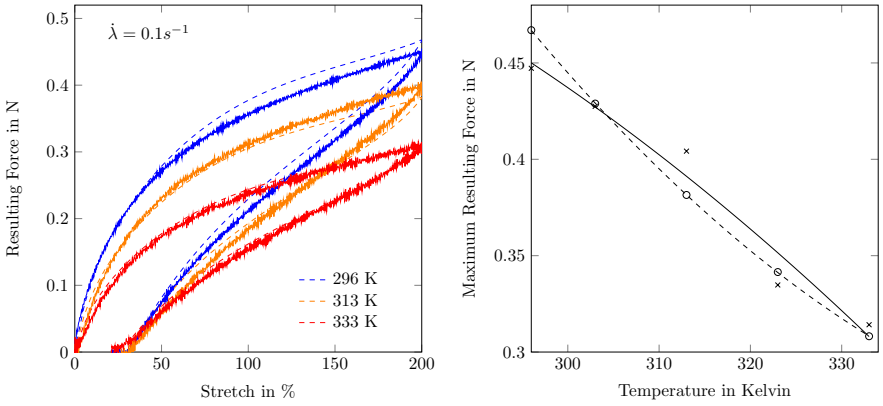

Fig. 8 Simulation results meet with experimental data where the data are obtained from cyclic loading tests performed at different temperatures. (Left) Simulation (dashed lines) and experimental values (marks) over the applied stretch. (Right) Simulation (o-marks and dashed trend line) and experimental values (x-marks and solid line) of the resulting force for the maximum applied stretch over the temperature range for the strain rate of 0.1 s^{-1}.

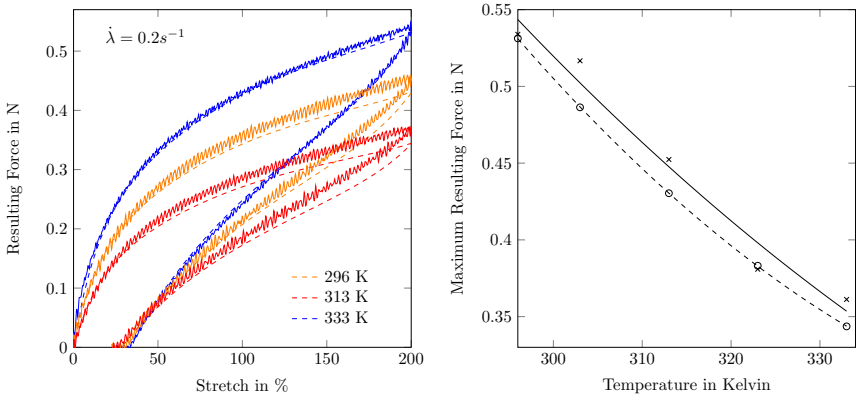

Fig. 9 Simulations meet with experiments, in which experimental data are extracted from cyclic loading tests conducted at different temperatures. (left) Simulation (dashed lines) and experimental values (marks) over the applied stretch. (right) Simulation (o-marks and dashed trend line) and experimental values (x-marks and solid line) of the resulting force for the maximum applied stretch over the temperature range for the strain rate of 0.2 s^{-1}.

necessary, as the entire finite element simulation has to be run separately for each iteration of the optimization, which results in a significant computational burden.
With this we find the values of the material parameters, introduced for the coupling of the elastic and the viscous energy as $\beta^e = 3.0791 \cdot 10^{-12}$ N/(Vmm)^2, $\beta_1^v = 2.3974 \cdot 10^{-14}$ N/(Vmm)^2, $\beta_2^v = 2.7304 \cdot 10^{-14}$ N/(Vmm)^2, $\beta_3^v = 1.8847 \cdot 10^{-15}$ N/(Vmm)^2 and $\gamma_2 = 5.9777 \cdot 10^{-12}$N/V^2. The identified parameter values lead to a simulated material response as depicted in Figures 10 to 12. On the left-hand side the applied force over the entire cyclic loading experiment is plotted. The experimental

results are depicted as black circles for the purely mechanical case, i.e. a voltage difference of 0 kV, and as blue triangles for a potential difference of 6 kV. The dashed lines in the according color show the results from the FE simulation. The plots on the right-hand side depict the applied force for the maximum applied stretch of 200% over the applied voltages. Here, the experimental results are depicted as black squares, whereas the results from the simulation are depicted as red crosses. A dashed trend line is added for both the computational and the experimental results for purely representational purposes. Furthermore, the scaling of the y-axis is adjusted in such a way that the influence of the electric field can easily be identified.

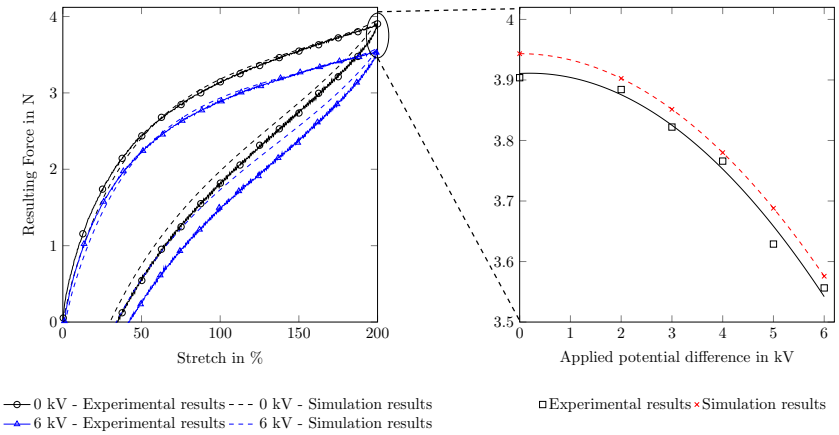

Fig. 10 Loading-unloading test for a strain rate of $\dot{\lambda} = 0.025\ \mathrm{s}^{-1}$. (Left) Applied force over the entire loading-unloading cycle. (Right) Applied force at the maximum stretch value for all applied potential differences.

Note that the constitutive model formulated in Section 3 can be fitted accurately with the experimental data that are obtained over the entire range of the applied strain for different applied voltage differences and strain rates. To quantify the quality of the fit, the coefficient of determination can be calculated. For the data presented in the left plots of Figures 10 to 12, the value of R^2 ranges between 0.9606 and 0.9913 demonstrating the high quality of the fit.

The remaining experimental data, i.e., the cyclic-loading tests conducted under an electric field and increased temperature, can be used as further validation of our model. It is assumed that the thermal and electric effects are superimposed without additional heating effects. Thus, we neglect possible heat generation effects that

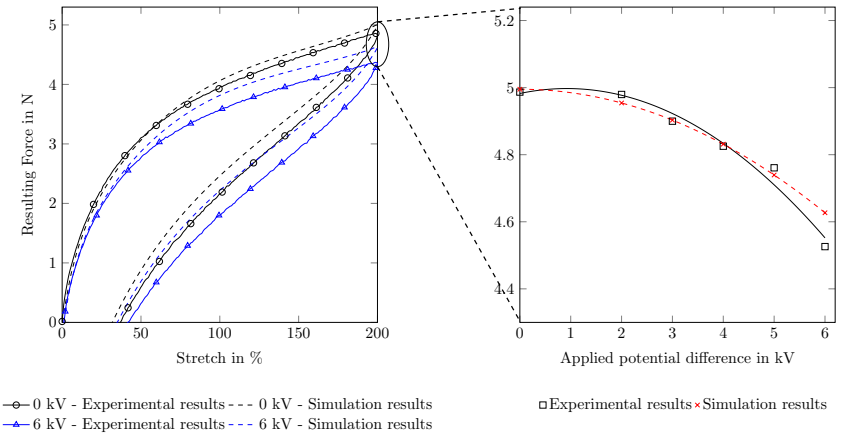

Fig. 11 Loading-unloading test for a strain rate of $\dot{\lambda} = 0.1\ \mathrm{s}^{-1}$. (Left) Applied force over the entire loading-unloading cycle. (Right) Applied force at the maximum strain value for all applied potential differences.

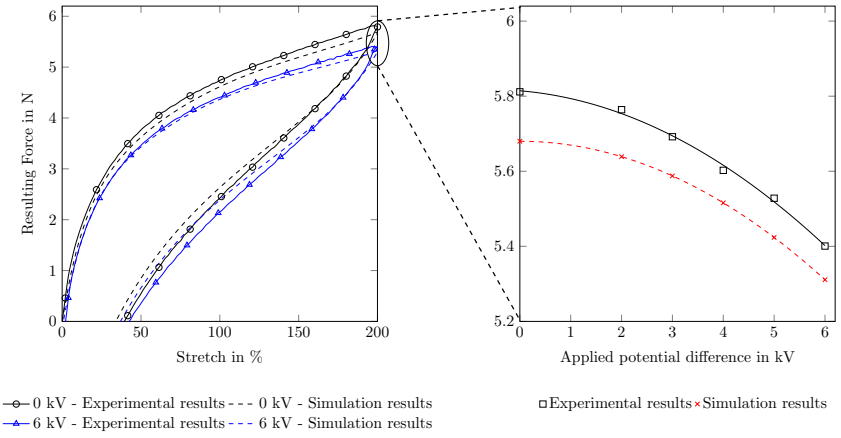

Fig. 12 Loading-unloading test for a strain rate of $\dot{\lambda} = 0.2\ \mathrm{s}^{-1}$. (Left) Applied force over the entire loading-unloading cycle. (Right) Applied force at the maximum strain value for all applied potential differences.

appear in the heat conduction equation (20). In the case of a temperature change due to the application of an electric field, this assumption is based on a lack of experimental evidence with adequate data sets. Possible heat generation due to the mechanical deformation is neglected due to the fact that the material is deformed under only a single cycle, which does not result in a considerable magnitude of the Gough-Joule effect. Furthermore, we assume that the coupling parameters are not explicitly dependent on temperature. A comparison between the results of the finite element simulation and the experimental data is depicted in Figure 13. The curves

show the results of the electro-mechanical tests at reference temperature and at an increased temperature of 55 °C for 0 kV and 6 kV.

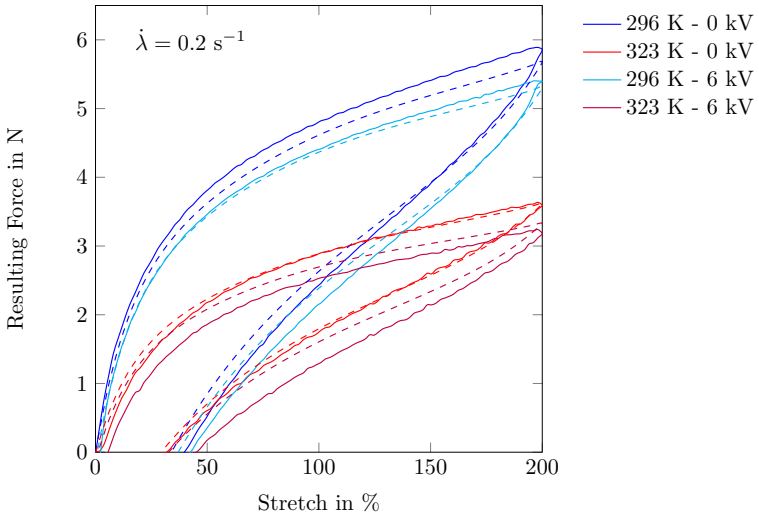

Fig. 13 Resulting force over the applied strain of cyclic loading tests at different temperatures and applied electric voltages. Experimental data plotted as solid lines, simulation results plotted as dashed lines.

The plots clearly show that the proposed modeling approach in combination with the identified material parameters is capable of correctly replicating the experimental behavior of VHB 4905$^{\mathrm{TM}}$ conducted under a combined thermo-electro-mechanical loading. With a unique set of identified material parameters, the thermo-electro-viscoelastic coupled model can match simulation results nicely with experimental data even for non-homogeneous deformation. To conclude the parameter identification, Table 2 summarizes the values for all material parameters.

5 Summary and outlook

In this contribution, a thermodynamically consistent numerical modelling approach for the simulation of dielectric elastomers under combined thermo-electro-mechanical loading was presented. The proposed model was specified for the highly viscous polymer VHB 4905$^{\mathrm{TM}}$. In combination with the cinorehensive experimental results presented in Part I, all relevant material parameters appearing in the constitutive model were identified in Part II. For the replication of the mechanical and thermo-mechanical experiments, analytical solutions were derived whereas in the

VHB 4905™				
Mechanical Base Parameters				
Elastic Parameters				
c_1^e	c_2^e	c_3^e		
0.015	$-5.97 \cdot 10^{-4}$	$3.15 \cdot 10^{-5}$		
Viscous Parameters				
μ_1^v	μ_2^v	μ_3^v		
$4.14 \cdot 10^{-3}$	$1.89 \cdot 10^{-2}$	$3.42 \cdot 10^{-3}$		
τ_1	τ_2	τ_3		
0.81	27.14	759.74		
Thermal Scaling Parameters				
a_1^e	a_2^e	a^v		
$7.64 \cdot 10^{-3}$	$-5.60 \cdot 10^{-5}$	4.69		
Electro-Mechanical Coupling Parameters				
β^e	γ_2	β_1^v	β_2^v	β_3^v
$3.08 \cdot 10^{-12}$	$5.98 \cdot 10^{-12}$	$2.40 \cdot 10^{-14}$	$2.73 \cdot 10^{-14}$	$1.88 \cdot 10^{-15}$

Table 2 Summary of the identified material parameters for VHB 4905™. Parameters c_i, μ_i^v in N/mm^2, τ_i in s, β^e, β_i^v in N/(Vmm)^2, $\hat{\gamma}_2$ in N/V^2.

case of an electric field, a finite-element implementation was used for the solution of the problem. In our future work, we aim to present a similar investigation for the characterization of polymers filled with piezoactive particles that will amplify the electro-mechanical coupling.

Acknowledgements:
M. Mehnert acknowledges the funding within the DFG project No. STE 544/52-2 and GRK2495/C. M. Hossain would like to extend his sincere appreciation to Engineering and Physical Sciences Research Council (EPSRC) for an Impact Acceleration Award (EP/R511614/1).

References

1. J. M. McCracken, B. R. Donovan, and T. J. White, "Materials as machines," *Advanced Materials*, vol. 32, no. 20, p. 1906564, 2020.
2. R. Pelrine, R. Kornbluh, and G. Kofod, "High-strain actuator materials based on dielectric elastomers," *Advanced Materials*, vol. 12, no. 16, pp. 1223–1225, 2000.
3. R. Pelrine, R. Kornbluh, Q. Pei, and J. Joseph, "High-speed electrically actuated elastomers with strain greater than 100%," *Science*, vol. 287, no. 5454, pp. 836–839, 2000.
4. F. Carpi, I. Anderson, S. Bauer, G. Frediani, G. Gallone, M. Gei, C. Graaf, C. Jean-Mistral, W. Kaal, G. Kofod, *et al.*, "Standards for dielectric elastomer transducers," *Smart Materials and Structures*, vol. 24, no. 10, p. 105025, 2015.
5. D. J. Griffiths, *Introduction to Electrodynamics, 2nd ed.* Englewood Cliffs: Prentice Hall, 1989.
6. J. D. Jackson, *Classical electrodynamics*. John Wiley & Sons, 2007.

7. A. C. Eringen, "On the foundations of electroelastostatics," *International Journal of Engineering Science*, vol. 1, no. 1, pp. 127–153, 1963.
8. R. A. Toupin, "The elastic dielectric," *Journal of Rational Mechanics and Analysis*, vol. 5, no. 6, pp. 849–915, 1956.
9. A. Kovetz, *Electromagnetic theory*. Oxford University Press Oxford, 2000.
10. G. A. Maugin, "On modelling electromagnetomechanical interactions in deformable solids," *International Journal of Advances in Engineering Sciences and Applied Mathematics*, vol. 1, no. 1, pp. 25–32, 2009.
11. J. Ericksen, "Theory of elastic dielectrics revisited.," *Archive for Rational Mechanics & Analysis*, vol. 183, no. 2, 2007.
12. G. A. Holzapfel and J. C. Simo, "A new viscoelastic constitutive model for continuous media at finite thermomechanical changes," *International Journal of Solids and Structures*, vol. 33, no. 20-22, pp. 3019–3034, 1996.
13. M. Kaliske and H. Rothert, "Formulation and implementation of three-dimensional viscoelasticity at small and finite strains," *Computational Mechanics*, vol. 19, no. 3, pp. 228–239, 1997.
14. J. C. Simo, "On a fully three-dimensional finite-strain viscoelastic damage model: formulation and computational aspects," *Computer methods in applied mechanics and engineering*, vol. 60, no. 2, pp. 153–173, 1987.
15. N. Huber and C. Tsakmakis, "Finite deformation viscoelasticity laws," *Mechanics of materials*, vol. 32, no. 1, pp. 1–18, 2000.
16. S. Reese and S. Govindjee, "A theory of finite viscoelasticity and numerical aspects," *International journal of solids and structures*, vol. 35, no. 26-27, pp. 3455–3482, 1998.
17. A. Ask, A. Menzel, and M. Ristinmaa, "Phenomenological modeling of viscous electrostrictive polymers," *International Journal of Non-Linear Mechanics*, vol. 47, no. 2, pp. 156–165, 2012.
18. A. Ask, A. Menzel, and M. Ristinmaa, "Electrostriction in electro-viscoelastic polymers," *Mechanics of Materials*, vol. 50, pp. 9–21, 2012.
19. J. D. Ferry, *Viscoelastic properties of polymers*. John Wiley & Sons, 1980.
20. A. Lion, *Thermomechanik von Elastomeren*. Institut für Mechanik, Universität Kassel, 2000.
21. T. Alts, *Thermodynamik elastischer Körper mit thermo-kinematischen Zwangsbedingungenfadenverstärkte Materialien*. Univ.-Bibl. d. Techn. Univ. Berlin, Abt. Publikationen, 1979.
22. R. Behnke, M. Kaliske, and M. Klüppel, "Thermo-mechanical analysis of cyclically loaded particle-reinforced elastomer components: experiment and finite element simulation," *Rubber Chemistry and Technology*, vol. 89, no. 1, pp. 154–176, 2016.
23. B. Dippel, M. Johlitz, and A. Lion, "Thermo-mechanical couplings in elastomers - experiments and modelling," *ZAMM-Journal of Applied Mathematics and Mechanics/Zeitschrift für Angewandte Mathematik und Mechanik*, vol. 95, no. 11, pp. 1117–1128, 2015.
24. A. Lion, "A physically based method to represent the thermo-mechanical behaviour of elastomers," *Acta Mechanica*, vol. 123, no. 1-4, pp. 1–25, 1997.
25. S. Reese and S. Govindjee, "Theoretical and numerical aspects in the thermo-viscoelastic material behaviour of rubber-like polymers," *Mechanics of Time-Dependent Materials*, vol. 1, no. 4, pp. 357–396, 1997.
26. R. Behnke and M. Kaliske, "The extended non-affine tube model for crosslinked polymer networks: Physical basics, implementation, and application to thermomechanical finite element analyses," in *Designing of Elastomer Nanocomposites: From Theory to Applications*, pp. 1–70, Springer, 2016.
27. M. Johlitz, D. Scharding, S. Diebels, J. Retka, and A. Lion, "Modelling of thermo-viscoelastic material behaviour of polyurethane close to the glass transition temperature," *ZAMM-Journal of Applied Mathematics and Mechanics/Zeitschrift für Angewandte Mathematik und Mechanik: Applied Mathematics and Mechanics*, vol. 90, no. 5, pp. 387–398, 2010.
28. L. Anand, N. M. Ames, V. Srivastava, and S. A. Chester, "A thermo-mechanically coupled theory for large deformations of amorphous polymers. part i: Formulation," *International Journal of Plasticity*, vol. 25, no. 8, pp. 1474–1494, 2009.

29. N. M. Ames, V. Srivastava, S. A. Chester, and L. Anand, "A thermo-mechanically coupled theory for large deformations of amorphous polymers. part ii: Applications," *International Journal of Plasticity*, vol. 25, no. 8, pp. 1495–1539, 2009.
30. S. Lu and K. Pister, "Decomposition of deformation and representation of the free energy function for isotropic thermoelastic solids," *International Journal of Solids and Structures*, vol. 11, no. 7-8, pp. 927–934, 1975.
31. A. Lion, "On the large deformation behaviour of reinforced rubber at different temperatures," *Journal of the Mechanics and Physics of Solids*, vol. 45, no. 11, pp. 1805–1834, 1997.
32. P. Erbts and A. Düster, "Accelerated staggered coupling schemes for problems of thermoelasticity at finite strains," *Computers & Mathematics with Applications*, vol. 64, no. 8, pp. 2408–2430, 2012.
33. M. Mehnert, M. Hossain, and P. Steinmann, "On nonlinear thermo-electro-elasticity," *Proceedings of the Royal Society A: Mathematical, Physical and Engineering Sciences*, vol. 472, no. 2190, p. 20160170, 2016.
34. F. Vogel, S. Göktepe, P. Steinmann, and E. Kuhl, "Modeling and simulation of viscous electroactive polymers," *European Journal of Mechanics-A/Solids*, vol. 48, pp. 112–128, 2014.
35. J.-P. Pelteret and P. Steinmann, *Magneto-Active Polymers: Fabrication, characterisation, modelling and simulation at the micro-and macro-scale*. Walter de Gruyter GmbH & Co KG, 2019.
36. D. Vu, "A study on nonlinear electro-elastostatics: Theory and numerical simulation," *Habilitation, Friedrich-Alexander University of Erlangen-Nürnberg: Erlangen, Bayern, Germany*, 2014.
37. B. D. Coleman and W. Noll, "The thermodynamics of elastic materials with heat conduction and viscosity," *Archive for Rational Mechanics and Analysis*, vol. 13, no. 1, pp. 167–178, 1963.
38. A. Dorfmann and R. Ogden, "Magnetoelastic modelling of elastomers," *European Journal of Mechanics-A/Solids*, vol. 22, no. 4, pp. 497–507, 2003.
39. A. Dorfmann and R. Ogden, "Nonlinear magnetoelastic deformations of elastomers," *Acta Mechanica*, vol. 167, no. 1, pp. 13–28, 2004.
40. M. Mehnert, M. Hossain, and P. Steinmann, "Numerical modeling of thermo-electro-viscoelasticity with field-dependent material parameters," *International Journal of Non-Linear Mechanics*, vol. 106, pp. 13–24, 2018.
41. O. H. Yeoh, "Some forms of the strain energy function for rubber," *Rubber Chemistry and technology*, vol. 66, no. 5, pp. 754–771, 1993.
42. P. Steinmann, M. Hossain, and G. Possart, "Hyperelastic models for rubber-like materials: consistent tangent operators and suitability for treloar's data," *Archive of Applied Mechanics*, vol. 82, no. 9, pp. 1183–1217, 2012.
43. M. Mehnert and P. Steinmann, "On the influence of the compliant electrodes on the mechanical behavior of vhb 4905," *Computational Materials Science*, vol. 160, pp. 287–294, 2019.
44. N. Koprowski-Theiss, M. Johlitz, and S. Diebels, "CHARACTERIZING THE TIME DEPENDENCE OF FILLED EPDM," *Rubber Chemistry and Technology*, vol. 84, pp. 147–165, 06 2011.
45. M. Mehnert, T. Mathieu-Pennober, and P. Steinmann, "On the influence of the coupled invariant in thermo-electro-elasticity," in *Generalized Models and Non-classical Approaches in Complex Materials 1*, pp. 533–554, Springer, 2018.
46. M. Mehnert, M. Hossain, and P. Steinmann, "Experimental and numerical investigations of the electro-viscoelastic behavior of vhb 4905tm," *European Journal of Mechanics-A/Solids*, vol. 77, p. 103797, 2019.
47. Z. Liao, M. Hossain, X. Yao, M. Mehnert, and P. Steinmann, "On thermo-viscoelastic experimental characterization and numerical modelling of vhb polymer," *International Journal of Non-Linear Mechanics*, vol. 118, p. 103263, 2020.
48. M. Johlitz, S. Diebels, and W. Possart, "Investigation of the thermoviscoelastic material behaviour of adhesive bonds close to the glass transition temperature," *Archive of Applied Mechanics*, pp. 1–14, 2012.
49. A. Ask, A. Menzel, and M. Ristinmaa, "Modelling of viscoelastic dielectric elastomers with deformation dependent electric properties," *Procedia Iutam*, vol. 12, pp. 134–144, 2015.

50. P. Saxena, D. K. Vu, and P. Steinmann, "On rate-dependent dissipation effects in electro-elasticity," *International Journal of Non-Linear Mechanics*, vol. 62, pp. 1–11, 2014.
51. D. Bishara and M. Jabareen, "A solid–shell formulation based on the assumed natural inhomogeneous strains for modeling the viscoelastic response of electro-active polymers," *Computational Mechanics*, vol. 66, no. 1, pp. 1–25, 2020.
52. P. Steinmann, "Computational nonlinear electro-elasticity - getting started -," in *Mechanics and Electrodynamics of Magneto-and Electro-elastic Materials*, pp. 181–230, Springer, 2011.
53. A. Dorfmann and R. Ogden, "Nonlinear electroelasticity," *Acta Mechanica*, vol. 174, no. 3-4, pp. 167–183, 2005.
54. M. Hossain, D. K. Vu, and P. Steinmann, "Experimental study and numerical modelling of vhb 4910 polymer," *Computational Materials Science*, vol. 59, pp. 65–74, 2012.
55. C. Linder, M. Tkachuk, and C. Miehe, "A micromechanically motivated diffusion-based transient network model and its incorporation into finite rubber viscoelasticity," *Journal of the Mechanics and Physics of Solids*, vol. 59, no. 10, pp. 2134–2156, 2011.
56. A. Amin, M. Alam, and Y. Okui, "An improved hyperelasticity relation in modeling viscoelasticity response of natural and high damping rubbers in compression: experiments, parameter identification and numerical verification," *Mechanics of materials*, vol. 34, no. 2, pp. 75–95, 2002.
57. A.-W. Hamkar and S. Hartmann, "Theoretical and numerical aspects in weak-compressible finite strain thermo-elasticity," *Journal of Theoretical and Applied Mechanics*, vol. 50, pp. 3–22, 2012.
58. L. R. G. Treloar, *The physics of rubber elasticity*. Oxford University Press, USA, 1975.
59. P. Haupt and C. Tsakmakis, "On the application of dual variables in continuum mechanics," *Continuum Mechanics and Thermodynamics*, vol. 1, no. 3, pp. 165–196, 1989.
60. A. Spencer, "Part iii. theory of invariants," *Continuum physics*, vol. 1, pp. 239–353, 2013.
61. C.-C. Wang, "A new representation theorem for isotropic functions: An answer to professor gf smith's criticism of my papers on representations for isotropic functions," *Archive for rational mechanics and analysis*, vol. 36, no. 3, pp. 166–197, 1970.
62. R. Bustamante, "Transversely isotropic non-linear electro-active elastomers," *Acta mechanica*, vol. 206, no. 3-4, p. 237, 2009.
63. L. Dorfmann and R. W. Ogden, "Nonlinear electroelasticity: material properties, continuum theory and applications," in *Proc. R. Soc. A*, vol. 473, p. 20170311, The Royal Society, 2017.
64. F. Vogel, *On the Modeling and Computation of Electro-and Magneto-active Polymers*. Lehrstuhl für Technische Mechanik, Universität Erlangen-Nürnberg, 2015.
65. R. Bustamante, "A variational formulation for a boundary value problem considering an electro-sensitive elastomer interacting with two bodies," *Mechanics Research Communications*, vol. 36, no. 7, pp. 791–795, 2009.
66. R. Bustamante, "Transversely isotropic nonlinear magneto-active elastomers," *Acta mechanica*, vol. 210, no. 3-4, pp. 183–214, 2010.
67. D. L. Henann, S. A. Chester, and K. Bertoldi, "Modeling of dielectric elastomers: Design of actuators and energy harvesting devices," *Journal of the Mechanics and Physics of Solids*, vol. 61, no. 10, pp. 2047–2066, 2013.
68. G. A. Holzapfel and R. W. Ogden, "Constitutive modelling of arteries," in *Proceedings of the Royal Society of London A: Mathematical, Physical and Engineering Sciences*, vol. 466, pp. 1551–1597, The Royal Society, 2010.
69. J. Merodio and R. Ogden, "Material instabilities in fiber-reinforced nonlinearly elastic solids under plane deformation," *Archives of Mechanics*, vol. 54, no. 5-6, pp. 525–552, 2002.
70. L. Dorfmann and R. W. Ogden, *Nonlinear mechanics of soft fibrous materials*. Springer, 2014.
71. M. Elahinia, R. Vertechy, G. Berselli, V. Parenti Castelli, and M. Bergamasco, "Continuum thermo-electro-mechanical model for electrostrictive elastomers," *Journal of Intelligent Material Systems and Structures*, vol. 24, no. 6, pp. 761–778, 2013.
72. P. Chadwick, "Thermo-mechanics of rubberlike materials," *Philosophical Transactions of the Royal Society of London A: Mathematical, Physical and Engineering Sciences*, vol. 276, no. 1260, pp. 371–403, 1974.

73. G. Holzapfel and J. Simo, "Entropy elasticity of isotropic rubber-like solids at finite strains," *Computer Methods in applied mechanics and engineering*, vol. 132, no. 1-2, pp. 17–44, 1996.
74. J. Nowinski and B. Boley, "Theory of thermoelasticity with applications," *Journal of Applied Mechanics*, vol. 47, p. 459, 1980.

6 Appendix

6.1 Considerations for incompressible materials under non-isothermal conditions

The aim of our modeling approach is to simulate a material that exhibits incompressible behavior at constant temperatures but is able to undergo a volumetric deformation due to thermal loading. Following the concept outlined in [57], the deformation gradient is split multiplicatively into a thermal contribution $\boldsymbol{F}_\Theta$ and an electro-mechanical contribution $\boldsymbol{F}_{EM}$, which may be interpreted as the introduction of an intermediate configuration termed herein as $\mathcal{B}_{EM}$, c.f. Figure 1. While the thermal deformation is purely volumetric, the electro-mechanical deformation may, in general, contain isochoric and volumetric contributions. Consequently, the deformation is described by

$$\boldsymbol{F} = \boldsymbol{F}_\Theta \boldsymbol{F}_{EM} = \boldsymbol{F}_\Theta \boldsymbol{F}_{EM}^{\text{iso}} \boldsymbol{F}_{EM}^{\text{vol}}. \tag{40}$$

The introduction of the volume changing electro-mechanical deformation $\boldsymbol{F}_{EM}^{\text{vol}}$ and the volume preserving deformation $\boldsymbol{F}_{EM}^{\text{iso}}$ motivates the introduction of the isochoric right Cauchy-Green tensor $\overline{\boldsymbol{C}}_{EM} = J_{EM}^{-2/3} \boldsymbol{C}_{EM}$ that is based on the Jacobian $J_{EM} = \det(\boldsymbol{F}_{EM})$ and the regular right Cauchy-Green tensor $\boldsymbol{C}_{EM} = \boldsymbol{F}_{EM}^T \boldsymbol{F}_{EM}$. When we assume isotropic thermal expansion, e.g. described by a linear formulation in the form $J_\Theta = 1 + \alpha[\Theta - \Theta_0]$ [58], where α is the thermal expansion coefficient, the thermal deformation gradient can be formulated as

$$\boldsymbol{F}_\Theta = J_\Theta^{\frac{1}{3}} \boldsymbol{I} \rightarrow \boldsymbol{C}_\Theta = J_\Theta^{\frac{2}{3}} \boldsymbol{I}. \tag{41}$$

Here a right Cauchy-Green tensor $\boldsymbol{C}_\Theta$ is introduced that corresponds to the thermal expansion. Additionally we introduce the Green strain tensors as

$$\begin{aligned}
\boldsymbol{E} &= \frac{1}{2}[\boldsymbol{F}^T \boldsymbol{F} - \boldsymbol{I}] = \frac{1}{2}[\boldsymbol{C} - \boldsymbol{I}], \\
\boldsymbol{E}_{EM} &= \frac{1}{2}[\boldsymbol{F}_{EM}^T \boldsymbol{F}_{EM} - \boldsymbol{I}] = \frac{1}{2}[\boldsymbol{C}_{EM} - \boldsymbol{I}], \\
\boldsymbol{E}_\Theta &= \boldsymbol{E} - \boldsymbol{E}_{EM} = \frac{1}{2}[\boldsymbol{F}^T \boldsymbol{F} - \boldsymbol{F}_{EM}^T \boldsymbol{F}_{EM}] = \frac{1}{2}[\boldsymbol{F}_\Theta^T \boldsymbol{F}_\Theta - \boldsymbol{I}].
\end{aligned} \tag{42}$$

Noteably, the multiplicatively decomposition of the deformation gradient leads to an additive decomposition of the Green strain, which becomes especially visible in

Equation $(43)_1$. These can be transformed into their counterparts $\boldsymbol{\Gamma}$, $\boldsymbol{\Gamma}_{EM}$ and $\boldsymbol{\Gamma}_{\Theta}$ in the electro-mechanical intermediate configuration by a push forward operation leading to

$$\begin{aligned}
\boldsymbol{\Gamma} &= \boldsymbol{F}_{EM}^{-T}\boldsymbol{E}\boldsymbol{F}_{EM}^{-1} = \boldsymbol{\Gamma}_{EM} + \boldsymbol{\Gamma}_{\Theta},\\
\boldsymbol{\Gamma}_{EM} &= \boldsymbol{F}_{EM}^{-T}\boldsymbol{E}_{EM}\boldsymbol{F}_{EM}^{-1} = \frac{1}{2}[\boldsymbol{I} - \boldsymbol{F}_{EM}^{-T}\boldsymbol{F}_{EM}^{-1}],\\
\boldsymbol{\Gamma}_{\Theta} &= \boldsymbol{F}_{EM}^{-T}\boldsymbol{E}_{\Theta}\boldsymbol{F}_{EM}^{-1} = \boldsymbol{F}_{EM}^{-T}\frac{1}{2}[\boldsymbol{F}^{T}\boldsymbol{F} - \boldsymbol{F}_{EM}^{T}\boldsymbol{F}_{EM}]\boldsymbol{F}_{EM}^{-1}\\
&= \frac{1}{2}[\boldsymbol{F}_{\Theta}^{T}\boldsymbol{F}_{\Theta} - \boldsymbol{I}] = \boldsymbol{E}_{\Theta}.
\end{aligned} \tag{43}$$

It should be noted that the push forward of $\boldsymbol{E}_{\Theta}$ results in an identical expression $\boldsymbol{\Gamma}_{\Theta}$, which is inevitable, as the Green Strain $\boldsymbol{E}_{\Theta}$ is located in the intermediate configuration by definition. Next we derive the strain-rate tensor $\overset{\triangle}{\boldsymbol{\Gamma}}$ of the combined deformation relative to the intermediate configuration that reads

$$\overset{\triangle}{\boldsymbol{\Gamma}} = \boldsymbol{F}_{EM}^{-T}\dot{\boldsymbol{E}}\boldsymbol{F}_{EM}^{-1} = \dot{\boldsymbol{\Gamma}} + \boldsymbol{L}_{EM}^{T}\boldsymbol{\Gamma} + \boldsymbol{\Gamma}\boldsymbol{L}_{EM} = \overset{\triangle}{\boldsymbol{\Gamma}}_{EM} + \overset{\triangle}{\boldsymbol{\Gamma}}_{\Theta}, \tag{44}$$

with the velocity gradient $\boldsymbol{L}_{EM} = \dot{\boldsymbol{F}}_{EM}\boldsymbol{F}_{EM}^{-1}$. The time derivative of the intermediate electro-mechanical and thermal strains take the form

$$\begin{aligned}
\overset{\triangle}{\boldsymbol{\Gamma}}_{EM} &= \boldsymbol{F}_{EM}^{-T}\dot{\boldsymbol{E}}_{EM}\boldsymbol{F}_{EM}^{-1} = \dot{\boldsymbol{\Gamma}}_{EM} + \boldsymbol{L}_{EM}^{T}\boldsymbol{\Gamma}_{EM} + \boldsymbol{\Gamma}_{EM}\boldsymbol{L}_{EM}\\
&= \frac{1}{2}[\boldsymbol{L}_{EM} + \boldsymbol{L}_{EM}^{T}],\\
\overset{\triangle}{\boldsymbol{\Gamma}}_{\Theta} &= \boldsymbol{F}_{EM}^{-T}\dot{\boldsymbol{E}}_{\Theta}\boldsymbol{F}_{EM}^{-1} = \dot{\boldsymbol{\Gamma}}_{\Theta} + \boldsymbol{L}_{EM}^{T}\boldsymbol{\Gamma}_{\Theta} + \boldsymbol{\Gamma}_{\Theta}\boldsymbol{L}_{EM}.
\end{aligned} \tag{45}$$

Thus, with the expressions given in Equations (41) and (43), we can derive $\dot{\boldsymbol{\Gamma}}_{\Theta}$ as

$$\dot{\boldsymbol{\Gamma}}_{\Theta} = \frac{1}{3}J_{\Theta}^{-\frac{1}{3}}\frac{\partial J_{\Theta}}{\partial \Theta}\dot{\Theta}\boldsymbol{I}, \tag{46}$$

whereas $\overset{\triangle}{\boldsymbol{\Gamma}}_{\Theta}$ can be expressed as

$$\overset{\triangle}{\boldsymbol{\Gamma}}_{\Theta} = \dot{\boldsymbol{\Gamma}}_{\Theta} + [J_{\Theta}^{\frac{2}{3}} - 1]\overset{\triangle}{\boldsymbol{\Gamma}}_{EM}. \tag{47}$$

We now introduce an appropriate stress measure $\boldsymbol{S}^{\mathrm{tot}}$, a Piola-Kirchhoff type stress, as a work conjugate to the Green strain. Within the concept of a specific stress power p [59] this leads to

$$p = \boldsymbol{S}^{\mathrm{tot}} : \dot{\boldsymbol{E}} = \boldsymbol{S}^{\mathrm{tot}} : [\boldsymbol{F}_{EM}^{T}\overset{\triangle}{\boldsymbol{\Gamma}}\boldsymbol{F}_{EM}] = \boldsymbol{S}_{EM}^{\mathrm{tot}} : \overset{\triangle}{\boldsymbol{\Gamma}} = \boldsymbol{S}_{EM}^{\mathrm{tot}} : [\overset{\triangle}{\boldsymbol{\Gamma}}_{\Theta} + \overset{\triangle}{\boldsymbol{\Gamma}}_{EM}], \tag{48}$$

where the intermediate stress $\boldsymbol{S}_{EM}^{\mathrm{tot}}$ is introduced as the push-forward of $\boldsymbol{S}^{\mathrm{tot}}$ to the intermediate configuration. With Equation (47) this can be transformed to

$$p = \boldsymbol{S}^{\text{tot}}_{EM} : [\dot{\boldsymbol{\Gamma}}_\Theta + [J_\Theta^{\frac{2}{3}} - 1]\overset{\triangle}{\boldsymbol{\Gamma}}_{EM} + \overset{\triangle}{\boldsymbol{\Gamma}}_{EM}] = \boldsymbol{S}^{\text{tot}}_{EM} : [\dot{\boldsymbol{\Gamma}}_\Theta + J_\Theta^{\frac{2}{3}}\overset{\triangle}{\boldsymbol{\Gamma}}_{EM}]. \tag{49}$$

We can now incorporate $\boldsymbol{S}^{\text{tot}}_{EM}$ into the Clausius-Planck inequality (14), which results in

$$\begin{aligned} &-\dot{\Omega} - \dot{\Theta}H + \boldsymbol{S}^{\text{tot}} : \dot{\boldsymbol{E}} - \dot{\mathbb{E}}\mathbb{D} \geq 0, \\ &-\dot{\Omega} - \dot{\Theta}\, H + \boldsymbol{S}^{\text{tot}}_{EM} : [\dot{\boldsymbol{\Gamma}}_\Theta + J_\Theta^{\frac{2}{3}}\overset{\triangle}{\boldsymbol{\Gamma}}_{EM}] - \dot{\mathbb{E}}\mathbb{D} \geq 0. \end{aligned} \tag{50}$$

Using the definition of $\dot{\boldsymbol{\Gamma}}_\Theta$ given in Equation (46) this can further be transformed into

$$-\dot{\Omega} + \dot{\Theta}\left[\frac{1}{3}J_\Theta^{-\frac{1}{3}}\frac{\partial J_\Theta}{\partial \Theta}\boldsymbol{S}^{\text{tot}}_{EM} : \boldsymbol{I} - H\right] + J_\Theta^{\frac{2}{3}}\boldsymbol{S}^{\text{tot}}_{EM} : \overset{\triangle}{\boldsymbol{\Gamma}}_{EM} - \mathbb{P}\dot{\mathbb{E}} \geq 0. \tag{51}$$

Now we can formulate an augmented free energy function Ω parameterized in terms of $\boldsymbol{C}_{EM}$, Θ and $\mathbb{E}$, which results in a time derivative in the form

$$\dot{\Omega}(\boldsymbol{C}_{EM}, \Theta, \mathbb{E}) = \frac{\partial \Omega(\boldsymbol{C}_{EM}, \Theta, \mathbb{E})}{\partial \boldsymbol{C}_{EM}} : \dot{\boldsymbol{C}}_{EM} + \frac{\partial \Omega(\boldsymbol{C}_{EM}, \Theta, \mathbb{E})}{\partial \Theta}\dot{\Theta} + \frac{\partial \Omega(\boldsymbol{C}_{EM}, \Theta, \mathbb{E})}{\partial \mathbb{E}}\dot{\mathbb{E}}. \tag{52}$$

Thus, if we recall $\dot{\boldsymbol{C}}_{EM} = 2\dot{\boldsymbol{E}}_{EM} = 2\boldsymbol{F}^T_{EM}\overset{\triangle}{\boldsymbol{\Gamma}}_{EM}\boldsymbol{F}_{EM}$, Equations (51) and (52) can be combined resulting in the constitutive equations for the intermediate stress, the entropy and the electric displacement

$$\boldsymbol{S}^{\text{tot}}_{EM} = 2J_\Theta^{-\frac{2}{3}}\boldsymbol{F}_{EM}\frac{\partial \Omega}{\partial \boldsymbol{C}_{EM}}\boldsymbol{F}^T_{EM}, \quad \mathbb{D} = -\frac{\partial \Omega}{\partial \mathbb{E}}, \quad H = \frac{1}{3}J_\Theta^{-\frac{1}{3}}\frac{\partial J_\Theta}{\partial \Theta}\boldsymbol{S}^{\text{tot}} : \boldsymbol{C}_{EM} - \frac{\partial \Omega}{\partial \Theta}. \tag{53}$$

In the subsequent calculations, the stress in the reference configuration is used frequently, which can be derived by a simple pull-back operation of the intermediate stress resulting in the expression

$$\boldsymbol{S}^{\text{tot}} = \boldsymbol{F}^{-1}_{EM}\boldsymbol{S}^{\text{tot}}_{EM}\boldsymbol{F}^{-T}_{EM} = 2J_\Theta^{-\frac{2}{3}}\frac{\partial \Omega}{\partial \boldsymbol{C}_{EM}}. \tag{54}$$

The derived framework can be specified to correctly replicate the material response of a DE under thermo-electro-mechanical loading. For this, the energy function may be extended by, for instance, including internal variables in order to model the time-dependency of a viscoelastic material.

7 General framework for a coupled energy function

The aim of this appendix is the introduction of a suitable framework for the formulation of an energy function that correctly describes the response of a polymeric material experiencing a thermo-electro-mechanical loading. This framework will be derived step by step, beginning with the isothermal case. The information presented therein has been investigated as well in our previous publication [45] where,

in addition to mathematical formulations, a number of illustrative boundary value problems were presented. Subsequently, a thermodynamically consistent formulation for a thermally coupled energy function is derived. This is initially done under the assumption of a constant specific heat capacity, resulting in a linear scaling of the energy function with the temperature, which is also shown in [33]. In order to simulate a nonlinear dependency of the energy function on the temperature, in the next step, a more general form of the specific heat capacity is selected, leading to a generalized formulation, as presented in [40]. As the energy function is intended to be used for the simulation of polymeric materials that are typically incompressible, in a final step, special focus is put on ensuring that the energy function correctly describes incompressibility at constant temperatures while still replicating a thermal expansion.

7.1 Isothermal energy function

We will begin by investigating the case of an electro-mechanically coupled material, i.e., isotropic electro-elastic behavior without considering thermal influences. It is assumed that the material response can be derived from a corresponding energy function, referred to as the isothermal energy contribution. As shown in [36], the concept of isotropy is closely related to the theory of isotropic tensor functions. Thus, following the representation theorem [60, 61], a scalar-valued function $\mathcal{F} = \mathcal{F}(\mathbf{A}, \mathbf{b})$ is invariant with respect to the proper orthogonal group $SO(3)$ if and only if it can be expressed as a function of the six principal invariants of $\mathbf{A}$ and $\mathbf{b}$ [45], i.e.

$$\mathcal{F}(\mathbf{A}, \mathbf{b}) = \mathcal{F}(I_{1\mathbf{A}}, I_{3\mathbf{A}}, I_{3\mathbf{A}}, I_{4\mathbf{b}}, I_{5\mathbf{Ab}}, I_{6\mathbf{Ab}}). \tag{55}$$

Therefore, we introduce the energy function $\Psi_0(\mathbf{F}_{EM}, \mathbb{E})$ as a contribution to the free energy (13) in the form $\Psi(\boldsymbol{F}, \Theta, \mathbb{E}) = \Psi(\Psi_0(\boldsymbol{F}_{EM}, \mathbb{E}), \Theta)$. In the context of this work $\Psi_0(\mathbf{F}_{EM}, \mathbb{E})$ is best described as an energy contribution expressed in terms of a set of material parameters at reference temperature and is defined as an isotropic function depending on the electric field vector $\mathbb{E}$ and the right Cauchy-Green tensor $\boldsymbol{C}_{EM}$, which is valid based on the *principle of objectivity* [36]. Following e.g. [53, 36, 60], the first three invariants I_1, I_2, I_3 depend solely on the right Cauchy-Green tensor and are, therefore, purely mechanical quantities

$$I_1 = \operatorname{tr}(\mathbf{C}_{EM}), \qquad I_2 = \frac{1}{2}\Big[[\operatorname{tr}(\mathbf{C}_{EM})]^2 - \operatorname{tr}(\mathbf{C}_{EM}{}^2)\Big], \qquad I_3 = \det(\mathbf{C}_{EM}). \tag{56}$$

On the other hand, the purely electric fourth invariant I_4 reads

$$I_4 = [\mathbb{E} \otimes \mathbb{E}] : \mathbf{I}, \tag{57}$$

which is the definition of the electric field strength in the undeformed configuration. Throughout the literature, the form of the first four invariants is consistent, see for

example [62, 63, 18, 51]. However, for the form of the two remaining invariants I_5, I_6 that describe the coupling between the electric field and the mechanical deformation, two different options can be found. In various contributions [18, 64, 36, 65, 66, 67], the coupled invariants depend directly on the right Cauchy-Green tensor in the form

$$I_5 = [\mathbb{E} \otimes \mathbb{E}] : \mathbf{C}_{EM}, \qquad I_6 = [\mathbb{E} \otimes \mathbb{E}] : \mathbf{C}_{EM}^2. \tag{58}$$

A physical interpretation of these invariants can be found as well, though it is not as straight forward as the interpretation of I_4. As shown in [53], the electric field in the context of electro-elasticity introduces a behavior that is comparable to the preferred direction of a transversely isotropic material. Thus, we may consider the electric field as the normal vector to an area-like quantity, analogously to the size of an area element $\mathrm{d}A$ in the material configuration and $\mathrm{d}a$ in the spatial configuration. As presented in [68], this leads to the notion that I_5 is a measure of the changes of this area-like quantity, normal to the electric field, multiplied with the electric field strength in the deformed configuration, i.e., the ratio $\frac{\mathrm{d}a^2}{\mathrm{d}A^2}|\mathfrak{e}|^2$.
Alternatively, the inverse of the right Cauchy-Green tensor can be used for the definition of a different version of the coupling invariants as presented for example in [53, 68, 69, 70]. This alternative formulation will be labeled $\widetilde{I_5}$, $\widetilde{I_6}$ in the context of this work and takes the form

$$\widetilde{I_5} = [\mathbb{E} \otimes \mathbb{E}] : \mathbf{C}_{EM}^{-1}, \qquad \widetilde{I_6} = [\mathbb{E} \otimes \mathbb{E}] : \mathbf{C}_{EM}^{-2}. \tag{59}$$

In this formulation the fifth invariant can intuitively be interpreted as the square of the electric field strength in the deformed configuration, i.e.

$$\widetilde{I_5} = [\mathbb{E} \otimes \mathbb{E}] : \mathbf{C}_{EM}^{-1} = \mathbb{E}\mathbf{C}_{EM}^{-1}\mathbb{E}^T = |\mathfrak{e}|^2. \tag{60}$$

Both of these formulations are invariant to the proper orthogonal group $SO(3)$ and are therefore valid options for the formulation of the coupling invariants of a free energy function of an isotropic material. In the context of this work, we will restrict ourselves to the initial formulation based directly on the right Cauchy-Green tensor. The interested reader is referred to [45] for a more detailed insight into the differences between the two formulations. It should be noted however that, even though the selection of an energy function that contains the coupling invariants I_5 or I_6 in general results in a connection between the electric field and the mechanical response, it does not necessarily mean that it correctly replicates the behavior of a dielectric elastomer under the loading of an electric field. Therefore, the effects of material parameters that are sensitive to an electric field were thoroughly investigated in [40].

7.2 Thermally coupled energy function

7.2.1 Constant heat capacity

The electro-mechanically coupled energy contribution derived in the previous chapter will now be integrated into a framework that introduces the temperature as an additional field. To this end, we follow the approach presented by Reese and Govindjee [25] and adapted it to electro-mechanics. As a starting point, the Legendre transformation as given in Equation (13) is used, which reads

$$\Psi(\boldsymbol{F}, \Theta, \mathbb{E}) = \mathcal{U} - \Theta H - \mathbb{E}\mathbb{P} = \mathcal{U} + \Theta \frac{\partial \Omega}{\partial \Theta} - \mathbb{E}\mathbb{P} = \mathcal{U} + \Theta \frac{\partial \Psi}{\partial \Theta} - \mathbb{E}\mathbb{P}. \tag{61}$$

Here we have made the use of the constitutive equation for the entropy as given in (17). For the sake of readability and in order to abbreviate the expressions, the free energy is labelled as Ψ in the following. When the derivative of this function with respect to the temperature is taken, we find that

$$\frac{\partial \Psi}{\partial \Theta} = \frac{\partial \mathcal{U}}{\partial \Theta} + \frac{\partial \Psi}{\partial \Theta} + \underbrace{\Theta \frac{\partial^2 \Psi}{\partial \Theta \partial \Theta}}_{-c} \longrightarrow \frac{\partial \mathcal{U}}{\partial \Theta} \quad = c. \tag{62}$$

Here we use the definition of the specific heat capacity c as found for example in [71, 72, 73, 31]. Consequently, the internal energy may be expressed depending on the specific heat capacity and the internal energy $\mathcal{U}_0$ at the reference temperature as

$$\mathcal{U} = \int_{\Theta_0}^{\Theta} c \, \mathrm{d}\widetilde{\Theta} + \mathcal{U}_0. \tag{63}$$

Based on the definition of the specific heat capacity

$$c = -\Theta \frac{\partial^2 \Psi}{\partial \Theta \partial \Theta}, \tag{64}$$

the derivative of the free energy with respect to the temperature takes the form

$$\frac{\partial \Psi}{\partial \Theta} = \int_{\Theta_0}^{\Theta} -\frac{c}{\widetilde{\Theta}} \mathrm{d}\widetilde{\Theta} + \left. \frac{\partial \Psi}{\partial \Theta} \right|_{\Theta_0}. \tag{65}$$

By inserting Equations (63) and (65) into (61), the free energy can be expressed as

$$\begin{aligned} \Psi &= \int_{\Theta_0}^{\Theta} c \, \mathrm{d}\widetilde{\Theta} + \mathcal{U}_0 + \Theta \left[\int_{\Theta_0}^{\Theta} -\frac{c}{\widetilde{\Theta}} \mathrm{d}\widetilde{\Theta} + \left. \frac{\partial \Psi}{\partial \Theta} \right|_{\Theta_0} \right] - \mathbb{E}\mathbb{P} \\ &= \mathcal{U}_0 + \Theta \left. \frac{\partial \Psi}{\partial \Theta} \right|_{\Theta_0} + \int_{\Theta_0}^{\Theta} c \left[1 - \frac{\Theta}{\widetilde{\Theta}} \right] \mathrm{d}\widetilde{\Theta} - \mathbb{E}\mathbb{P}. \end{aligned} \tag{66}$$

Based on Equation (61), the derivative of the free energy with respect to the temperature, evaluated at the reference temperature can be expressed as

$$\Psi_0 = \mathcal{U}_0 + \Theta_0 \left.\frac{\partial \Psi}{\partial \Theta}\right|_{\Theta_0} - \mathbb{E}\mathbb{P} \longrightarrow \Theta \left.\frac{\partial \Psi}{\partial \Theta}\right|_{\Theta_0} = \frac{\Theta}{\Theta_0}[\Psi_0 - \mathcal{U}_0 + \mathbb{E}\mathbb{P}], \tag{67}$$

which renders Equation (66) into the format

$$\Psi = \frac{\Theta}{\Theta_0}\Psi_0 + [\mathcal{U}_0 - \mathbb{E}\mathbb{P}]\left[1 - \frac{\Theta}{\Theta_0}\right] + \int_{\Theta_0}^{\Theta} c\left[1 - \frac{\Theta}{\widetilde{\Theta}}\right] \mathrm{d}\widetilde{\Theta}. \tag{68}$$

When the specific heat capacity at constant deformation and electric field is assumed to be temperature independent, i.e. $c|_{\boldsymbol{F},\mathbb{E}}(\Theta) = c|_{\boldsymbol{F},\mathbb{E}}(\Theta_0) = c_0$, this leads to

$$\Psi = \frac{\Theta}{\Theta_0}\Psi_0 + [\mathcal{U}_0 - \mathbb{E}\mathbb{P}]\left[1 - \frac{\Theta}{\Theta_0}\right] + c_0\left[\Theta - \Theta_0 - \Theta \ln\left(\frac{\Theta}{\Theta_0}\right)\right]. \tag{69}$$

Thus, for a constant specific heat capacity, the isothermal energy contribution Ψ_0 is scaled linearly by the temperature. The derived framework of a thermo-electro-mechanical energy function leads to a similar result as presented in [33, 40], in which the thermal coupling was derived following a slightly different approach. In order to maintain the structure of the energy functions presented therein, the term connected to the internal energy $\mathcal{U}_0$ is interpreted as the volumetric deformation due to thermal expansion, which is in accordance with the literature, see e.g. [25]. The remaining contribution $\mathbb{E}\mathbb{P}\left[1 - \frac{\Theta}{\Theta_0}\right]$ indicates a coupling between the electric field and the temperature and is combined with the first term on the right-hand side to the expression $\widetilde{\Psi}_0 = \frac{\Theta}{\Theta_0}\Psi_0 - \mathbb{E}\mathbb{P}\left[1 - \frac{\Theta}{\Theta_0}\right]$, resulting in the final form of the energy function

$$\Psi = \frac{\Theta}{\Theta_0}\widetilde{\Psi}_0 + c_0\left[\Theta - \Theta_0 - \Theta \ln\left(\frac{\Theta}{\Theta_0}\right)\right] - [\Theta - \Theta_0]M(\boldsymbol{F}_\Theta). \tag{70}$$

The specific form of $M(\boldsymbol{F}_\Theta)$ can be taken from literature, e.g. as $M(\boldsymbol{F}_\Theta) = 3\kappa_0\alpha_0 \ln(J_\Theta)$ with the bulk modulus κ_0 and the thermal expansion coefficient α_0.

7.2.2 Temperature dependent heat capacity

The calculations in the previous section have shown that the assumption of a temperature-independent specific heat capacity inevitably leads to a linear scaling of the free energy Ψ_0. However, it is well documented that the mechanical material parameters of various materials exhibit a nonlinear dependency on the temperature [58, 74]. Thus, as Ψ_0 is interpreted as an energy function containing a set of parameters of the material at the reference temperature, a more generalized form of the specific heat capacity has to be introduced. Following the approach presented in [25], we assume a base heat capacity c_0 that is amended by the free energy multiplied

by a temperature dependent scaling function in the form

$$c_{\boldsymbol{F},\mathbb{E}}(\Theta) = c_0 - \Theta \frac{\partial^2 g(\Theta)}{\partial \Theta^2} \widetilde{\Psi}_0. \tag{71}$$

When this formulation is introduced into Equation (68), the definition of the free energy function takes the form

$$\Psi = \frac{\Theta}{\Theta_0} \widetilde{\Psi}_0 + \mathcal{U}_0 \left[1 - \frac{\Theta}{\Theta_0} \right] + \int_{\Theta_0}^{\Theta} \left[c_0 - \widetilde{\Theta} \frac{\partial^2 g(\widetilde{\Theta})}{\partial \widetilde{\Theta}^2} \widetilde{\Psi}_0 \right] \left[1 - \frac{\Theta}{\widetilde{\Theta}} \right] \mathrm{d}\widetilde{\Theta}. \tag{72}$$

The integral on the right-hand side can be evaluated using partial integration, which results in the expression

$$\begin{aligned} \Psi =& \frac{\Theta}{\Theta_0} \widetilde{\Psi}_0 + \mathcal{U}_0 \left[1 - \frac{\Theta}{\Theta_0} \right] + c_0 \left[\Theta - \Theta_0 - \Theta \ln \left(\frac{\Theta}{\Theta_0} \right) \right] \\ &+ \left[g(\Theta) - g(\Theta_0) + \left. \frac{\partial g(\Theta)}{\partial \Theta} \right|_{\Theta_0} [\Theta - \Theta_0] \right] \widetilde{\Psi}_0. \end{aligned} \tag{73}$$

Eventually, the thermally coupled energy function takes the final form

$$\Psi = f(\Theta) \widetilde{\Psi}_0 + \mathcal{U}_0 \left[1 - \frac{\Theta}{\Theta_0} \right] + c_0 \left[\Theta - \Theta_0 - \Theta \ln \left(\frac{\Theta}{\Theta_0} \right) \right], \tag{74}$$

where the scaling of the energy function is summarized as

$$f(\Theta) = \frac{\Theta}{\Theta_0} + g(\Theta) - g(\Theta_0) + \left. \frac{\partial g(\Theta)}{\partial \Theta} \right|_{\Theta_0} [\Theta - \Theta_0]. \tag{75}$$

It should be noted that in general the base specific heat capacity may itself also depend on temperature, as presented for example in [26]. As the intention of the selected format of the specific heat capacity, as introduced in Equation (71), is the option of a nonlinear scaling of the material parameters, this alternative is not investigated further in the context of this work.